Journal of Volcanology and Geothermal Research 200 (2011) 171–191

Contents lists available at ScienceDirect

Journal of Volcanology and Geothermal Research

journal homepage: www.elsevier.com/locate/jvolgeores

# Petrology of the Luingo caldera (SE margin of the Puna plateau): A middle Miocene window of the arc–back arc configuration

S. Guzmán [a,*], I.A. Petrinovic [b], J.A. Brod [c], F.D. Hongn [a], R.E. Seggiaro [a], C. Montero [a,d], R. Carniel [e], E.L. Dantas [f], M. Sudo [d]

[a] IBIGEO (CONICET-UNSa), Museo de Ciencias Naturales, Universidad Nacional de Salta, Mendoza 2, 4400, Salta, Argentina
[b] CICTERRA-FCEFyN, Universidad Nacional de Córdoba, Av. Vélez Sarsfield 1611, X5016GCA, Córdoba, Argentina
[c] IESA/UFG, Instituto de Estudos Sócio-Ambientais, Campus Samambaia, Caixa Postal 131-74001-970, Goiânia, Goiás, Brazil
[d] Universität Potsdam, Institut für Erd- und Umweltwissenschaften, Karl-Liebknecht-Strasse 24, 14476 Potsdam, Germany
[e] Laboratorio di misure e trattamento dei segnali, DIEA, Università di Udine, Via delle Scienze 208, 33100 Udine, Friuli, Italy
[f] Laboratorio de Geocronologia, Universidade de Brasília, Campus Asa Norte, 70.910-900 Brasília, Brazil

ARTICLE INFO

*Article history:*
Received 15 September 2010
Accepted 11 December 2010
Available online 22 December 2010

*Keywords:*
Luingo caldera
Central Andes
Miocene volcanism
Southern Central Volcanic Zone
crustal thickness

ABSTRACT

We describe the petrographic characteristics, whole-rock geochemistry and mineral chemistry of rocks from the Pucarilla–Cerro Tipillas Volcanic Complex with emphasis on the rocks belonging to the middle Miocene Luingo caldera, located in the south-eastern portion of the Central Volcanic Zone (CVZ) of the Andes. We modelled the petrogenesis of the Luingo caldera rocks as a mixture of ca. 20% crustal magmas and 80% of mantle magmas by AFC with recharge processes. A comparison of Luingo geochemical data with the composition of Miocene–Pliocene volcanic rocks from the broad area, points to major thickening events during the middle Miocene for the western portion and during the upper Miocene for the eastern portion of the Southern CVZ. In the eastern sector (~66°W) the mantle source appears to change from a spinel–lherzolite type for the middle Miocene to a garnet-lherzolite type for the upper Miocene-Pliocene magmas. The areal distribution of the volcanic products led to the recognition of approximately equivalent areas covered by volcanic rocks both in the eastern and in the western Puna borders. This indicates a broad arc, which was structurally controlled at the proto-Puna/Puna margins, whose geochemical differences are related with variations in crustal thicknesses and heterogeneous mantle sources from west to east.



## 1. Introduction

The Central Volcanic Zone (CVZ) of the Central Andes is developed between 14 and 28°S (Thorpe et al., 1984; de Silva and Francis, 1991) and is characterized by abundant Miocene to Recent ignimbrites, lavas and subvolcanic igneous bodies (e.g., Baker and Francis, 1978). The CVZ includes the Altiplano–Puna Volcanic Complex (APVC; de Silva, 1989) between 21 and 24°S, where large volumes of ignimbrites and abundant calderas were interpreted as the result of an "ignimbrite flare-up" (de Silva, 1989), bringing the region to the focus of various subsequent studies (e.g., de Silva, 1989; Ort et al., 1993; Lindsay et al., 2001a,b; Soler et al., 2007; Petrinovic et al., 2010). The APVC ignimbrites are predominantly crystal-rich calc-alkaline dacites (e.g., Harmon et al., 1984; de Silva and Francis, 1989; Soler et al., 2007). In contrast, the ignimbrites of the Southern CVZ (SCVZ, 25–27°S) have few detailed studies and a small number of recognized volcanic centres. In the western portion (between 67 and 69°W) they are characterized by small to medium volume (<10 $km^3$), crystal-poor ignimbrites of felsic compositions (e.g., Siebel et al., 2001; Schnurr et al., 2007); whereas to the east, the Cerro Galán caldera (e.g., Sparks et al., 1985) and the recently identified Luingo caldera (Guzmán and Petrinovic, 2008) have larger volumes and crystal-rich dacitic to rhyodacitic compositions as most of the ignimbrites of the APVC.

Luingo is the oldest (13–12 Ma; Guzmán and Petrinovic, 2010) and south-easternmost caldera recognized so far in the SE Puna plateau margin, in the transition with the Pampean Ranges. In the present article we describe the petrography, mineral chemistry and geochemistry of the Luingo volcanic rocks in order to characterize their composition and magmatic evolution.

The location of the Luingo caldera, close to the well known Cerro Galán caldera, provides an excellent opportunity to investigate their possible genetic relationship as suggested earlier by González et al. (1999) and Hongn and Seggiaro (2001). Furthermore, the Luingo caldera becomes a key area to understand possible variations in magma source and composition before and after the major thickening event (ca. 10 Ma: Isacks, 1988) occurred in this sector of the Puna.

* Corresponding author. Museo de Ciencias Naturales, Mendoza No. 2 (4400), Salta, Argentina. Tel./fax: +54 387 431 8086.
*E-mail addresses:* sguzman@unsa.edu.ar, sguzman@conicet.gov.ar (S. Guzmán).

0377-0273/$ – see front matter © 2010 Elsevier B.V. All rights reserved.
doi:10.1016/j.jvolgeores.2010.12.008

Finally, we compare the Luingo rocks with coeval ignimbrites and lavas located to the west in order to identify the possible middle Miocene arc–back arc configuration of the Southern CVZ.

## 2. Geological background

The Altiplano–Puna plateau results from the convergence between the South-American and Nazca plates (Isacks, 1988; Allmendinger et al., 1997; Riller and Oncken, 2003). An outstanding feature of this plateau is its large crustal thickness (e.g., Yuan et al., 2000; 2002), which has been attributed to the combined effect of horizontal shortening (Allmendinger, 1986; Isacks, 1988; Allmendinger and Gubbels, 1996; Allmendinger et al., 1997), magmatic addition (Allmendinger, 1986; Marrett and Emerman, 1992; Allmendinger et al., 1997), lithospheric thinning and hydration of the upper mantle (e.g., Allmendinger et al., 1997), underplating of the Brazilian Shield below the Altiplano and Northern Puna during the late Miocene (e.g., Allmendinger et al., 1986; Gubbels et al., 1993; Allmendinger et al., 1997; Sempere et al., 1997; Riller and Oncken, 2003) and weather variations that led to differences in the sedimentation rates (e.g., Riller and Oncken, 2003; Strecker et al., 2007).

In the southern portion of the CVZ, a group of pyroclastic deposits and minor lava flows, located immediately to the SE of the Cerro Galán caldera, were grouped in the Pucarilla–Cerro Tipillas Volcanic Complex (PCTVC; Guzmán and Petrinovic, 2008). The complex includes the middle Miocene Luingo caldera, which is the main subject of the present study. The Luingo caldera is set at the boundary between the Puna and the Eastern Cordillera and Pampean Ranges, where the crustal thickness is about 60 km (e.g., Heit et al., 2007). Luingo caldera marks the eastern limit of the large-volume Cenozoic magmatism of the Altiplano–Puna plateau.

Most of the Luingo caldera deposits are located in the southern extension of the Colomé–Hualfín Valley (Fig. 1) which is bounded by regional faults with opposite vergence. The western fault thrusts basement rocks onto the Payogastilla Group, whereas the eastern fault (Jasimaná Fault: Marrett et al., 1994) reflects a Neogene inversion of a previous normal fault (e.g., Seggiaro et al., 2006; Carrera and Muñoz, 2008) that marks the western limit of the Cretaceous Salta rift (e.g., Hongn and Seggiaro, 2001; Mortimer et al., 2007) and the eastern limit of the PCTVC. Other faults farther to the west have trends similar to the Jasimaná fault also with left-lateral oblique components and westward vergence (Guzmán, 2009). Some of these faults were active before and others after the Luingo eruptive event (Guzmán, 2009).

Units from the PCTVC unconformably cover lower Miocene fluvial sediments of the basal and middle sections of the Angastaco Formation (Marrett et al., 1994; Guzmán, 2009). In other sections, the PCTVC covers the local Neoproterozoic–Palaeozoic basement, including medium to high grade metamorphites, such as the La Paya Formation (Aceñolaza et al., 1976), the Río Blanco Metamorphic Complex (e.g., Hongn and Seggiaro, 2001) and the Loma Corral Formation (Navarro García, 1984), as well as granitoids of the Oire Eruptive Complex (Blasco and Zapettini, 1996) and the Peñas Blancas Granite (Castillo, 1999).

### 2.1. Volcanic units related to the Luingo caldera

Products from the Luingo caldera are mostly welded and devitrified ignimbrites and minor lavas. Their units, simplified stratigraphic relationships and available ages are summarized in Fig. 2. For a detailed description and discrimination of different units the reader is referred to Guzmán and Petrinovic (2010).

Pyroclastic units from the Luingo caldera comprise the Pucarilla and Alto de Las Lagunas ignimbrites (outflow units) and the Luingo I and Luingo II ignimbrites (intracaldera units); the latter two are separated from each other by a collapse breccia, the Luingo Breccia. The PCTVC lavas are separated in Lavas I (related to the Luingo caldera) and Lavas II (unrelated to the caldera). The Luingo caldera and related deposits are middle Miocene in age (Guzmán and Petrinovic, 2010; Fig. 2). New Laser-heating $^{40}Ar/^{39}Ar$ analyses of two biotite separates from Lava II have been obtained at the $^{40}Ar/^{39}Ar$ geochronology laboratory in the University of Potsdam, plateau ages yielded $7.59 \pm 0.03$ and $7.60 \pm 0.02$ Ma (see Appendix A for details). The bulk composition of the ignimbrites is dacitic, whereas Lavas I vary from trachyandesites to less common trachydacites and Lavas II are trachydacites.

Intracaldera facies (Luingo I and Luingo II ignimbrites) always show strong hydrothermal alteration, making it difficult to constrain the original composition and primary mineral association, thus major petrographic considerations were done in the outflow ignimbritic facies (Pucarilla and Alto de Las Lagunas ignimbrites) and lavas.

## 3. Petrography

The Pucarilla and Alto de Las Lagunas ignimbrites are pumice-rich (up to 40 vol.%), crystal-rich (between ca. 25 and 38 vol.% in pumices) and have low lithic contents (<3 vol.%). Three varieties (Fig. 3) of vesiculated fragments are recognized. The most common type (Fig. 3a, b) is white to black in hand specimen and grey to white in polarized light, the colour variations corresponding to different degrees of welding and devitrification. These vesiculated fragments are flattened to a variable extent as a function of the overall welding and compaction of the units. They are distinguished from the other two types by a generally coarser grain-size and by the common presence of clinopyroxene, both as phenocrysts and microphenocrysts and of titanite phenocrysts. Another pumice variety (<2%), is pink, typically flattened (Fig. 3c, d) and characterized by a large amount of broken and in some cases rounded crystals set in an aphanitic matrix where vesicles are overprinted by alteration and no longer recognizable; this type lacks titanite and only rarely contains clinopyroxene. A third variety of vesiculated clasts comprises grey crystal mush fragments (Fig. 3e, f), which are extremely crystal-rich (>90%), vesicle-poor and almost always sub-rounded, composed dominantly of plagioclase and biotite.

Both outflow ignimbrites (Alto de Las Lagunas and Pucarilla) contain plagioclase, biotite, magnetite, quartz, titanite, apatite and zircon; distinctively, the Pucarilla Ignimbrite also contains clinopyroxene whereas the Alto de Las Lagunas Ignimbrite has amphibole and scarce K-feldspar. All ignimbrites are fine- to medium-grained with an average phenocryst size of 2–3 mm occasionally reaching 6 mm. The Pucarilla Ignimbrite is divided in three units (Hualfín, Arremo and Jasimaná, from base to top) on the basis of variable devitrification and welding, and also of petrographic criteria, as detailed below.

The intracaldera ignimbrites (Luingo I and Luingo II) were strongly modified by post emplacement hydrothermal alteration. These are intensely welded ignimbrites in which flattened pumice fragments (up to 18 vol.%) are often difficult to recognize. They are crystal-rich (~35 vol.%), have low lithic contents (1–3 vol.%), and consist of variably altered plagioclase, clinopyroxene, biotite, quartz, apatite and titanite pseudomorphs with accessory Fe–Ti oxides and zircon and a variety of secondary minerals such as rutile, calcite, kaolinite, chlorite, sericite and epidote.

Lavas I are mostly trachyandesites with minor trachydacites. They are medium to fine grained and show porphyritic texture with a micro to cryptocrystalline intersertal and/or pilotaxic groundmass. Their mineral association consists of plagioclase, K-feldspar, clinopyroxene, with accessory apatite, Fe–Ti oxides ± biotite and titanite. Lavas II are fine to medium grained porphyritic dacites whose groundmass is either intersertal or pilotaxic and varies from microcrystalline to cryptocrystalline. They are composed of biotite, amphibole, plagioclase, quartz, Fe–Ti oxides ± clinopyroxene, orthopyroxene and titanite.

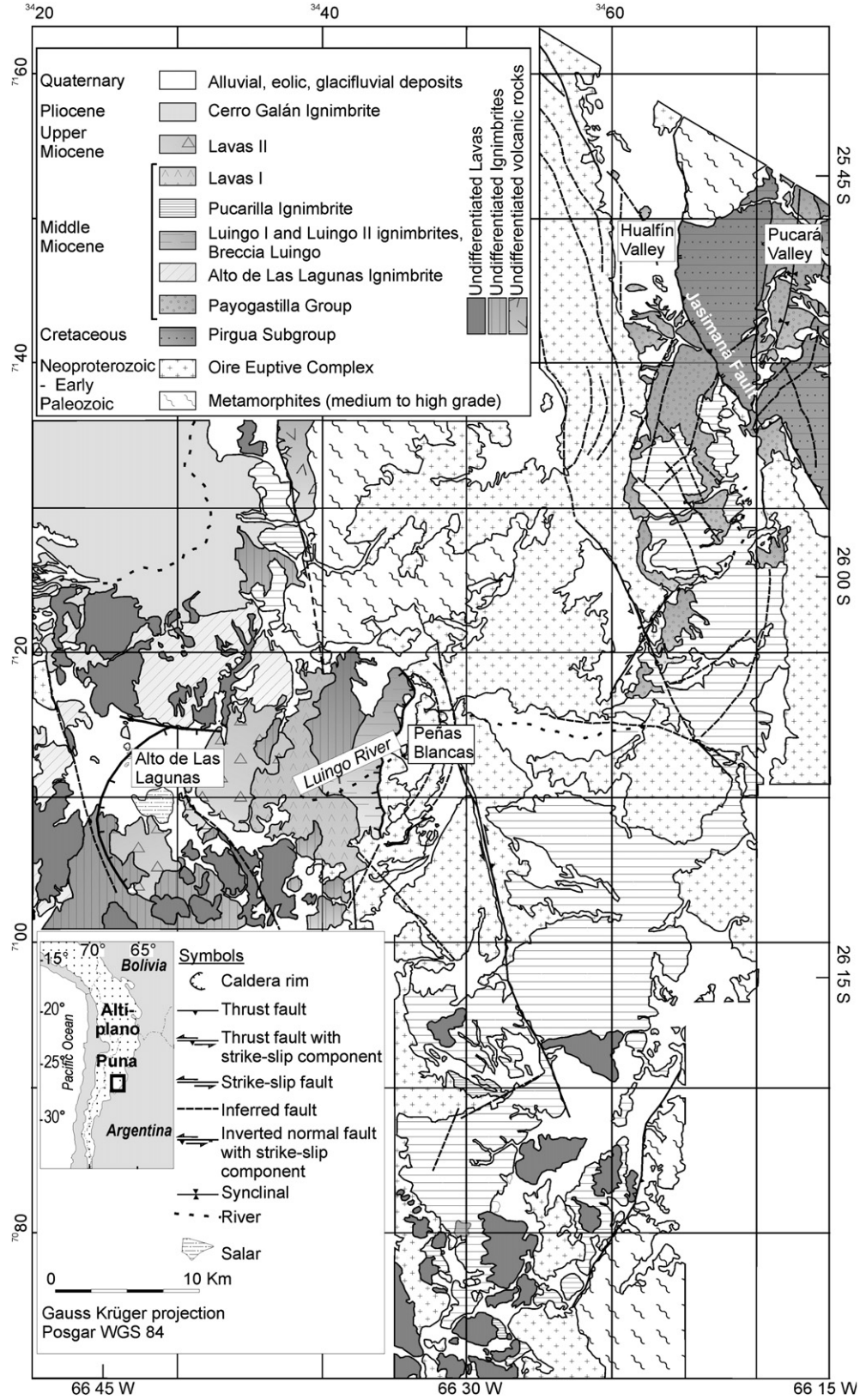


**Fig. 1.** Geologic map of the Pucarilla–Cerro Tipillas Volcanic Complex and the surrounding area. Modified from Guzmán and Petrinovic, 2010.

## 4. Mineral chemistry

Chemical analyses of selected minerals were performed by WDS with a Cameca SX-50 electron microprobe at the Institute of Geosciences, University of Brasilia, (see Appendix A for details). In the particular case of the ignimbrites, analyses were carried out only on grains located within pumice fragments, to minimize the possibility of contamination with xenocrystic material. In order to gain insights into chemical variation trends during crystal growth, analytical profiles were performed in selected individual crystals.

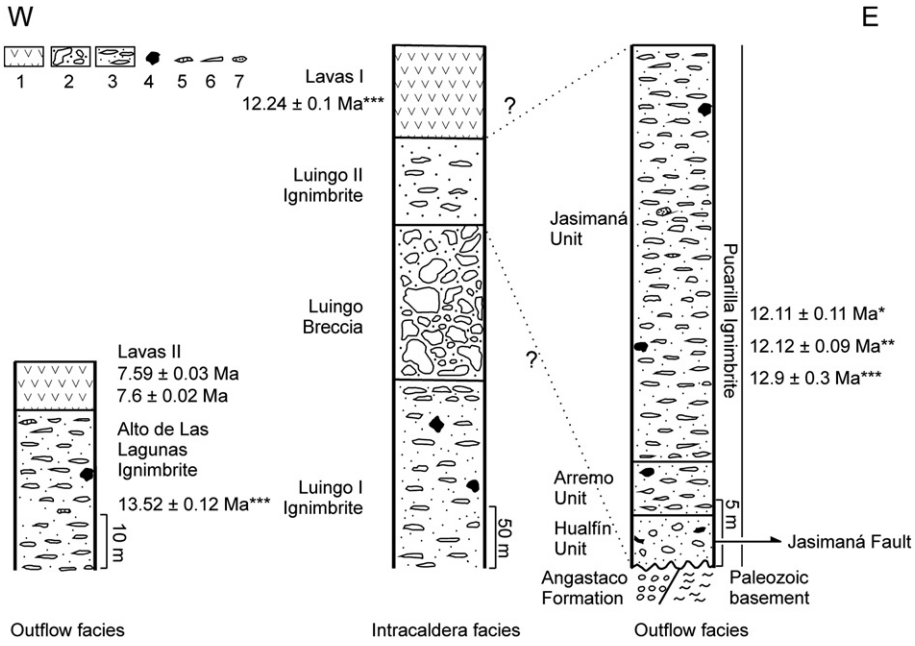


**Fig. 2.** Generalized sections of volcanic sequences from the PCTVC. 1) lavas, 2) breccias, 3) ignimbrites, 4) lithic fragments, 5) pink fiamme, 6) common fiamme/pumices, 7) grey crystal mush clasts. Ages are from this contribution and from *Marrett et al. (1994), **Folkes et al. (submitted for publication), *** Guzmán and Petrinovic, 2010. Modified from Guzmán and Petrinovic, 2010.

Representative chemical analyses of each mineral phase are shown in Tables 1–5, whereas the whole data set is represented in Figs. 4–8.

### 4.1. Pyroxene

Clinopyroxenes occur in the Pucarilla Ignimbrite and in the Lavas I and Lavas II units, but orthopyroxene is restricted to Lavas II. Representative analyses are given in Table 1. For classification and other diagrams, the cationic proportions were calculated on the basis of 6 oxygen and $Fe_2O_3$ was estimated according to the method of Droop (1987).

Clinopyroxene from the Pucarilla Ignimbrite occurs as 0.2 to 1.85 mm-long, subhedral, prismatic, often broken phenocrysts, locally forming glomerophyric aggregates. Many crystals are optically zoned, especially near the rims, which are often coated in Fe–Ti oxides. Common inclusions comprise apatite, with subordinate plagioclase, Fe–Ti oxides, and biotite.

In the Morimoto (1988) quadrilateral classification diagram (Fig. 4) they plot mostly as diopside ($Wo_{48-44}\ En_{41-34}\ Fs_{18-14}$). A single analysis (out of 93), belonging to a Jasimaná Unit pumice, plots in the augite field, with a minor calcic augite component. The fields for different ignimbrite and pumice types overlap widely, and there are no significant compositional differences between them. Data from single-crystal microprobe profiles reveal only narrow chemical zoning.

The pyroxene in the Lavas I Unit is calcic augite ($Wo_{44-39}\ En_{44-40}\ Fs_{18-13}$). Fig. 4 shows the compositional range, compared with the field of the Pucarilla Ignimbrite and the Lavas II pyroxenes. Analyzed grains from samples near the base of Lavas I Unit show normal zoning, whereas in those samples collected towards the top the zoning is both normal and reverse. Lavas II are the only unit where both clino and orthopyroxene are present (Fig. 4). The clinopyroxene is diopside ($Wo_{45.14\ -\ 46.46}$, $En_{38.53\ -\ 40.94}$, $Fs_{13.27\ -\ 15.55}$), it is almost unzoned, whereas the orthopyroxene shows reverse zoning and has a wide compositional variation ($Wo_{1.67-3.27}\ En_{60.65-79.95}\ Fs_{17.82-37.67}$).

### 4.2. Amphibole

Amphibole from the Alto de Las Lagunas Ignimbrite occurs as 0.05 to 2 mm-long crystals, they are subhedral to euhedral with tabular habit and are often coated in Fe–Ti oxides even becoming pseudomorphs. Lavas II amphiboles (0.1 to 1.25 mm) are subhedral to anhedral and frequently form glomerophyric aggregates.

For classification and other diagrams, cations were calculated on the basis of 23 O, and 2 (OH, F, Cl) groups. $Fe^{3+}$ was calculated as the average between minimum and maximum values as suggested by Leake et al. (1997). Since $(Ca+Na)_B \geq 1$ and $Na_B \leq 0.5$ for all analyses, they are classified as calcic amphiboles. Two subgroups were recognized on the basis of the parameters (a) $Ca_B \geq 1.5$, $(Na+K)_A \geq 0.5$, $Ti \leq 0.5$ and (b) $Ca_B \geq 1.5$, $(Na+K)_A \leq 0.5$, $Ca_A \leq 0.5$, and classified accordingly in the diagrams of Fig. 5(a) and (b) (Leake et al., 1997). Representative analyses are given in Table 2.

Amphiboles from the Alto de Las Lagunas Ignimbrite vary compositionally between alumino-edenite and alumino-magnesiohornblende. Crystals from the Lavas II Unit, on the other hand, show a wider composition range, encompassing alumino-edenite, alumino-pargasite, alumino-magnesiohornblende, and alumino-tschermakite.

Microprobe profiles in individual grains indicate that zoning in amphibole from the Alto de Las Lagunas Ignimbrite is very subtle and may be normal or reverse. In contrast, amphiboles from the Lavas II typically show reverse zoning, the rims being more Mg-rich and Al- and Ti-poor than the cores.

### 4.3. Biotite

Biotite (<0.05–2.95 mm) is subhedral with tabular to acicular habit; some crystals are bent and others show domino structure. It contains inclusions of iron–titanium oxides, apatite, plagioclase and zircon. Biotite crystals are often coated or even replaced by opaques due to vapour-phase alteration. Representative biotite analyses are given in Table 3. Chemical classification of the analyzed micas followed the recommendations in Tischendorf et al. (1997) and Yavutz (2001). $LiO_2$ content was estimated through the equation $Li_2O$ wt.% = 155*$(MgO)^{-3.1}$, for $SiO_2$ > 34 wt.% and MgO > 6 wt.%. All analyzed grains classify as Mg-biotite (Fig. 6), although it should be stressed that except for a few analyses, the micas in the Lavas I and Lavas II units are systematically richer in MgO (wt.%) than those in the ignimbrites. It is important to note that the presence of these MgO-rich biotites in the Pucarilla Ignimbrite may represent crystals that

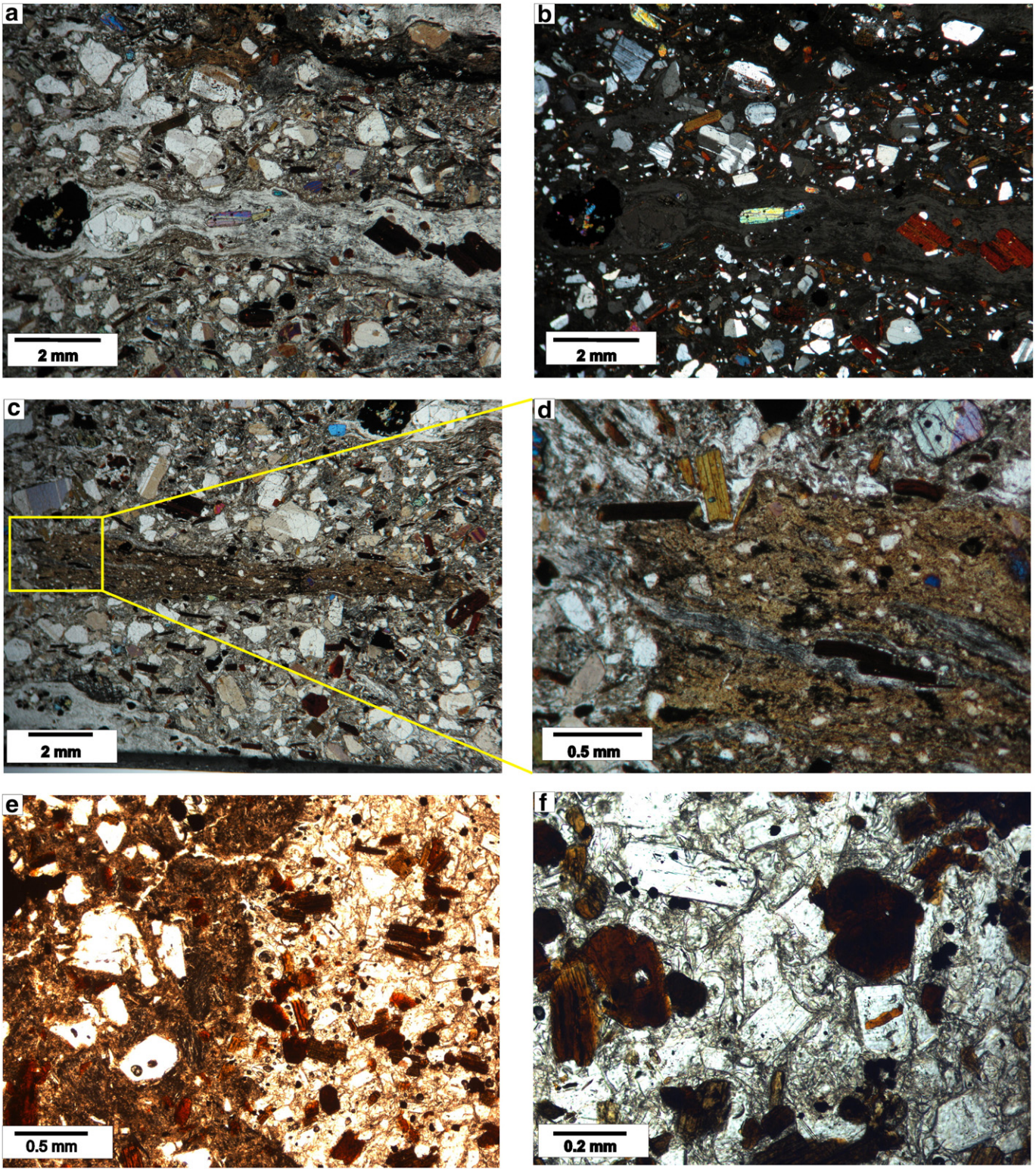


**Fig. 3.** Microphotographs of Luingo caldera's juvenile fragments. a, b) "common" pumice clasts, c, d) pink pumice type, in the detail photograph (d) it is seen that although the main fragment is of pink pumice, it is banded with the "common" type pumice; e, f) grey crystal mush clast to the right (e), and detail of that fragment (f).

belong to a magma batch of a different composition than the main one, as discussed latter in this paper.

Biotite from the pyroclastic sequences has high titanium content ($TiO_2$ wt.%: 4.12–5.13) similar to many other Puna ignimbrites (e.g., Vilama: Soler, 2005; Atana: Lindsay et al., 2001a) indicating relatively high pre-eruptive temperatures (c.f., Patiño Douce, 1993). $TiO_2$ content of biotite in the Lavas I Unit is even higher (5.39–5.82 wt.%), whereas biotite in Lavas II has $TiO_2$ contents in a range similar to the Pucarilla Ignimbrite. Biotites from the Alto de Las Lagunas Ignimbrite show the lowest $TiO_2$ content (4.12–4.53 wt.%), suggesting that these ignimbrites have the lowest pre-eruptive temperatures within the Luingo caldera ignimbrites. This is also in accordance with a typically

**Table 1**
Representative microprobe analyses of pyroxenes.

| Unit | Pucarilla Ignimbrite | | | | | | | | | | | | | | | Lavas I | | | | Lavas II | | | | | |
|---|---|---|---|---|---|---|---|---|---|---|---|---|---|---|---|---|---|---|---|---|---|---|---|---|---|
| | Hualfín Unit | | | | | Arremo Unit | | | | Jasimaná Unit | | | | | | | | | | | | | | | |
| Analysis | PAMP-06-6-1 | PAMP-06-6-2 | PAMP-06-6-3 | PAMP-06-8-2 | PAMP-06-8.3 | NO2-1-B5 | NO2-1-B6 | NO2-3-B1 | NO2-3-B2 | SN02-3-B3 | D04-1B-1 | D04-1B-2 | D04-1B-3 | PAMP-01-1-B1 | PAMP-01-1-B2 | PAMP-01-1-B3 | CMS21-1-B1 | CMS21-1-B2 | CMS18-4-B1 | CMS18-4B2 | CMS30-1-1 | CMS30-1-2 | CMS30-2-B1 | CMS30-2-B2 | CMS-30-2-3B |
| Position | Rim | Core | Rim | Core | Rim | Core | Rim | Rim | Core | Rim | Rim | Core | Rim | Rim | Core | Rim | Rim | Core | Rim | Core | Rim | Core | Rim | Core | Rim |
| | Pumice | Pumice | Pumice | | | Pumice | Pumice | Pumice | Pumice | Pumice | Pumice | Pumice | Pumice | Pumice | Pumice | Pumice | | | | | | | | | |
| Profile | 15.1 | 15.2 | 15.3 | 16.2 | 16.3 | 33.2 | 33.3 | 31.1 | 31.2 | 31.3 | 4.1 | 4.2 | 4.3 | 20.1 | 20.2 | 20.3 | 39.1 | 39.2 | 38.1 | 38.2 | 43.1 | 43.2 | 17.1 | 17.2 | 17.3 |
| $SiO_2$ | 52.73 | 53.25 | 52.18 | 53.35 | 53.88 | 51.89 | 52.46 | 52.94 | 52.48 | 52.07 | 52.69 | 53.21 | 53.15 | 52.54 | 52.37 | 51.95 | 52.09 | 52.28 | 49.20 | 49.91 | 52.57 | 49.19 | 52.14 | 52.22 | 52.55 |
| $TiO_2$ | 0.17 | 0.14 | 0.21 | 0.10 | 0.14 | 0.13 | 0.12 | 0.12 | 0.16 | 0.14 | 0.12 | 0.12 | 0.08 | 0.14 | 0.14 | 0.13 | 0.26 | 0.27 | 0.80 | 0.63 | 0.17 | 0.34 | 0.22 | 0.15 | 0.17 |
| $Al_2O_3$ | 1.18 | 0.66 | 1.56 | 0.94 | 1.01 | 0.99 | 0.77 | 0.82 | 0.90 | 0.81 | 1.07 | 0.95 | 0.84 | 0.94 | 0.98 | 0.88 | 1.60 | 1.54 | 3.77 | 3.15 | 2.29 | 7.02 | 1.25 | 0.89 | 1.10 |
| FeO | 9.33 | 7.88 | 9.17 | 8.38 | 8.32 | 8.61 | 8.24 | 8.33 | 8.95 | 8.07 | 8.82 | 7.90 | 8.11 | 8.77 | 9.23 | 8.15 | 9.39 | 9.13 | 9.43 | 8.26 | 12.46 | 18.53 | 9.18 | 8.64 | 8.92 |
| $Fe_2O_3$ | 0.01 | 0.16 | 0.35 | 0.16 | 0.35 | 0.00 | 0.00 | 0.00 | 0.01 | 0.00 | 0.06 | 0.41 | 0.05 | 0.00 | 0.00 | 0.00 | 0.00 | 0.01 | 0.01 | 0.00 | 0.01 | 0.01 | 0.00 | 0.00 | 0.00 |
| $Cr_2O_3$ | 0.04 | 0.00 | 0.00 | 0.04 | 0.00 | 0.03 | 0.02 | 0.01 | 0.00 | 0.02 | 0.03 | 0.00 | 0.02 | 0.00 | 0.01 | 0.00 | 0.02 | 0.02 | 0.01 | 0.03 | 0.76 | 0.16 | 0.02 | 0.00 | 0.02 |
| MnO | 0.82 | 0.87 | 0.91 | 0.91 | 0.90 | 0.84 | 0.79 | 0.65 | 0.84 | 0.89 | 0.98 | 0.94 | 0.95 | 0.76 | 0.88 | 0.84 | 0.63 | 0.63 | 0.34 | 0.28 | 0.18 | 0.33 | 0.64 | 0.76 | 0.63 |
| NiO | 0.00 | 0.05 | 0.00 | 0.03 | 0.00 | 0.07 | 0.01 | 0.04 | 0.01 | 0.04 | 0.02 | 0.00 | 0.00 | 0.00 | 0.00 | 0.09 | 0.00 | 0.00 | 0.00 | 0.04 | 0.03 | 0.00 | 0.03 | 0.00 | 0.00 |
| MgO | 13.86 | 13.98 | 12.28 | 13.41 | 13.63 | 13.49 | 14.15 | 13.84 | 14.66 | 14.13 | 13.47 | 13.10 | 14.18 | 14.16 | 13.56 | 14.36 | 15.39 | 15.07 | 14.79 | 15.26 | 28.41 | 22.74 | 13.85 | 14.35 | 14.18 |
| CaO | 22.01 | 22.55 | 22.09 | 23.05 | 22.44 | 23.06 | 22.97 | 22.91 | 22.36 | 22.79 | 22.49 | 22.59 | 22.55 | 22.08 | 22.18 | 22.46 | 20.87 | 20.77 | 20.69 | 21.52 | 1.19 | 1.57 | 22.38 | 22.46 | 22.42 |
| $Na_2O$ | 0.00 | 0.06 | 0.14 | 0.06 | 0.14 | 0.04 | 0.37 | 0.29 | 0.45 | 0.04 | 0.02 | 0.16 | 0.02 | 0.39 | 0.74 | 0.13 | 0.13 | 0.55 | 0.33 | 0.00 | 0.08 | 0.25 | 0.00 | 0.00 | 0.04 |
| $K_2O$ | 0.04 | 0.06 | 0.03 | 0.03 | 0.01 | 0.00 | 0.01 | 0.00 | 0.01 | 0.00 | 0.03 | 0.01 | 0.02 | 0.02 | 0.01 | 0.02 | 0.01 | 0.01 | 0.01 | 0.04 | 0.01 | 0.00 | 0.02 | 0.02 | 0.00 |
| Total | 100.17 | 99.66 | 98.92 | 100.45 | 100.83 | 99.14 | 99.91 | 99.95 | 100.83 | 99.00 | 99.80 | 99.39 | 99.97 | 99.78 | 100.10 | 99.01 | 100.39 | 100.28 | 99.36 | 99.13 | 98.17 | 100.12 | 99.72 | 99.48 | 100.03 |

**Table 2**
Representative microprobe analyses of amphiboles.

| Unit | Alto de Las Lagunas Ignimbrite | | | | Lavas II | | |
|---|---|---|---|---|---|---|---|
| Analysis | SCG4-4-A7 | SCG4-4-A8 | CMS-38-1-F1 | CMS-38-1-F2 | CMS28-1-A6 | CMS28-1-A5 | CMS28-1-A4 |
| | Pumice | Pumice | Pumice | Pumice | | | |
| Position | Core | Rim | Rim | Core | Rim | Core | Rim |
| $SiO_2$ | 46.06 | 46.09 | 45.25 | 45.21 | 46.04 | 42.78 | 47.13 |
| $TiO_2$ | 1.35 | 1.33 | 1.43 | 1.50 | 1.91 | 2.87 | 1.66 |
| $Al_2O_3$ | 8.22 | 8.02 | 8.59 | 8.91 | 8.47 | 11.39 | 8.08 |
| $Fe_2O_3$ | 2.61 | 4.55 | 4.24 | 2.33 | 4.14 | 3.90 | 5.37 |
| $Cr_2O_3$ | 0.04 | 0.02 | 0.00 | 0.02 | 0.01 | 0.00 | 0.06 |
| FeO | 12.50 | 11.25 | 12.31 | 14.03 | 8.93 | 8.89 | 7.94 |
| MnO | 0.70 | 0.67 | 0.76 | 0.73 | 0.31 | 0.15 | 0.34 |
| ZnO | 0.00 | 0.00 | 0.00 | 0.00 | 0.00 | 0.00 | 0.00 |
| MgO | 13.08 | 12.94 | 12.83 | 11.97 | 14.98 | 14.02 | 15.54 |
| CaO | 11.63 | 11.51 | 11.35 | 11.45 | 11.34 | 11.34 | 11.32 |
| $Na_2O$ | 1.78 | 1.09 | 1.92 | 2.06 | 1.65 | 1.88 | 1.48 |
| $K_2O$ | 0.96 | 1.02 | 1.148 | 1.084 | 0.88 | 1.06 | 0.78 |
| Total | 98.91 | 98.49 | 99.83 | 99.28 | 98.66 | 98.29 | 99.69 |

higher temperature association (biotite + pyroxene, with no amphibole) in the Pucarilla Ignimbrite than in the Alto de Las Lagunas Ignimbrite (amphibole + K feldspar) (c.f., Wones, 1970). Zoning in biotite is generally very subtle and in most cases it is normal.

### 4.4. Plagioclase

Plagioclase occurs in all studied units. In the Pucarilla Ignimbrite it often shows sieve texture, whereas embayments and corroded rims are rare. It also contains abundant inclusions, preferably located in zoning limits. Among these, apatite is conspicuous, biotite, zircon, and Fe–Ti oxides are less common and clinopyroxene is rare. Plagioclase from Luingo I and Luingo II ignimbrites is strongly altered to calcite and sericite. Plagioclase from the Lavas I and Lavas II units commonly shows corroded rims or intra-crystal disequilibrium features and sieve textures. Additionally, in Lavas I crystal growth under disequilibrium is apparent from plagioclase step zoning patterns.

Representative analyses are given in Table 4 and their classification in the Ab–Or–An diagram is shown in Fig. 7. Overall plagioclase composition in the outflow pyroclastic units varies from andesine to bytownite. In the intracaldera (Luingo I and Luingo II) ignimbrites plagioclase ranges from albite to oligoclase due to subsolidus alteration. These do not represent primary plagioclase, and will not be discussed here. Chemical zoning is common in plagioclase from all units, varying in intensity from prominent in the Arremo and Hualfin units to subtle in the Alto de Las Lagunas Ignimbrite.

Plagioclase from the Alto de Las Lagunas Ignimbrite has a composition restricted to andesine ($An_{45-31}$), does not show optical disequilibrium textures but shows zoning, both normal and reverse and locally oscillatory. Plagioclase from the Hualfín Unit varies from $An_{81}$ to $An_{33}$, is typically zoned towards lower An contents at the rims, with some detailed microprobe profiles suggesting the presence of step zoning. A grey crystal mush found in the Hualfín Unit and interpreted as an accidental lithic (although still related to Luingo caldera), contains two groups of plagioclase microlites: one varies from $An_{53}$ to $An_{35}$, but the other displays a much wider range ($An_{74-43}$) even within a single crystal. In the Arremo Unit, plagioclase varies from $An_{84}$ to $An_{32}$. Zoning patterns vary from normal, reverse, through oscillatory with strong evidence of mafic magma recharging (Fig. 8).

Plagioclase from the Jasimaná Unit ranges from $An_{64}$ to $An_{29}$. Specifically plagioclase in pink pumices has a more restricted range ($An_{46-33}$). Zoning patterns are both reverse and normal. Nevertheless, it is clear that the highest An % contents in the Jasimaná Unit plagioclase are found in the cores of normally-zoned crystals.

**Table 3**
Representative microprobe analyses of micas.

| Unit | Pucarilla Ignimbrite | | | | | | | | Alto de Las Lagunas Ignimbrite | | | Lavas I | | | Lavas II | |
|---|---|---|---|---|---|---|---|---|---|---|---|---|---|---|---|---|
| | Hualfín Unit | | Arremo Unit | | | Jasimaná Unit | | | | | | | | | | |
| Analysis | P007-1-D1 | P007-1-D2 | D07-1-D1 | D07-1-D2 | D07-1-D3 | D04-1-D1 | D04-1-D2 | D04-1-DE | CG4-4-D1 | CG4-4-D2 | CG4-4-D3 | CMS21-3-D1 | CMS21-3-D2 | CMS21-3-D3 | CMS28-1-D5 | CMS-281-D6 |
| | Pumice | Pumice | Pumice | Pumice | Pumice | Pumice | Pumice | Pumice | Pumice | Pumice | Pumice | | | | | |
| Position | Rim | Core | Rim | Core | Rim | Rim | Core | Rim | Rim | Core | Rim | Rim | Core | Rim | Core | Rim |
| $SiO_2$ | 36.79 | 36.58 | 37.79 | 37.43 | 37.73 | 36.58 | 37.45 | 37.13 | 36.00 | 36.69 | 36.31 | 36.88 | 36.48 | 37.05 | 37.28 | 37.39 |
| $TiO_2$ | 4.78 | 4.69 | 4.43 | 4.62 | 4.54 | 4.64 | 4.81 | 4.58 | 4.53 | 4.40 | 4.44 | 5.48 | 5.47 | 5.49 | 4.75 | 4.59 |
| $Al_2O_3$ | 13.35 | 13.31 | 13.20 | 13.54 | 13.49 | 13.60 | 13.52 | 13.47 | 13.91 | 13.62 | 13.86 | 13.65 | 13.61 | 13.72 | 13.92 | 13.71 |
| FeO | 16.44 | 16.49 | 15.96 | 16.07 | 15.58 | 16.39 | 16.02 | 16.15 | 18.22 | 17.79 | 17.49 | 11.88 | 15.07 | 13.53 | 13.74 | 13.30 |
| $Fe_2O_3$ | 0.48 | 0.78 | 0.00 | 0.47 | 0.00 | 0.10 | 0.06 | 0.00 | 0.26 | 0.20 | 0.00 | 1.01 | 0.94 | 0.70 | 0.51 | 0.36 |
| MnO | 0.32 | 0.32 | 0.27 | 0.22 | 0.44 | 0.23 | 0.30 | 0.26 | 0.41 | 0.28 | 0.36 | 0.12 | 0.23 | 0.16 | 0.09 | 0.12 |
| MgO | 13.55 | 13.50 | 13.75 | 14.70 | 13.63 | 13.77 | 14.03 | 13.75 | 12.59 | 13.24 | 12.87 | 16.18 | 14.38 | 15.54 | 16.02 | 16.22 |
| BaO | 0.00 | 0.00 | 0.00 | 0.00 | 0.00 | 0.00 | 0.05 | 0.00 | 0.03 | 0.00 | 0.00 | 0.15 | 0.38 | 0.00 | 0.09 | 0.18 |
| CaO | 0.10 | 0.03 | 0.14 | 0.00 | 0.08 | 0.00 | 0.00 | 0.00 | 0.00 | 0.00 | 0.02 | 0.01 | 0.00 | 0.00 | 0.00 | 0.01 |
| $Na_2O$ | 0.46 | 0.71 | 0.08 | 0.08 | 0.84 | 0.00 | 0.09 | 0.21 | 0.56 | 0.17 | 0.00 | 0.60 | 0.18 | 0.09 | 0.80 | 0.59 |
| $K_2O$ | 9.29 | 9.57 | 9.12 | 9.54 | 8.53 | 9.72 | 9.70 | 9.87 | 9.59 | 9.72 | 9.75 | 9.46 | 9.18 | 9.33 | 8.99 | 9.02 |
| Cl | 0.20 | 0.18 | 0.24 | 0.17 | 0.21 | 0.18 | 0.18 | 0.20 | 0.17 | 0.15 | 0.13 | 0.34 | 0.33 | 0.41 | 0.23 | 0.25 |
| $H_2O$ | 3.92 | 3.93 | 3.91 | 3.99 | 3.93 | 3.90 | 3.96 | 3.92 | 3.90 | 3.93 | 3.90 | 3.95 | 3.92 | 3.93 | 4.00 | 3.97 |
| SrO | 0.00 | 0.00 | 0.00 | 0.00 | 0.00 | 0.00 | 0.00 | 0.00 | 0.00 | 0.00 | 0.00 | 0.00 | 0.00 | 0.00 | 0.00 | 0.00 |
| Total | 99.68 | 100.08 | 98.88 | 100.84 | 98.99 | 99.11 | 100.16 | 99.56 | 100.16 | 100.19 | 99.12 | 99.72 | 100.17 | 99.96 | 100.40 | 99.71 |

Overall, An % content is distinctively higher in plagioclases of the Hualfín and Arremo units, in comparison with the Jasimaná Unit and the Alto de Las Lagunas Ignimbrite. It is noteworthy that some of the anorthite contents (up to 84 mol%) are significantly high for an overall dacitic system. It is possible that those Ca-rich plagioclases are related to recharge of the chamber with higher-temperature magmas and/or variations in pressure and volatile content (e.g., Streck, 2008).

In both outflow units of the Luingo caldera, there is a tendency for plagioclase cores from the pink pumices to have lower and more restricted (andesine) An contents than those in the grey crystal mush fragments or in the more abundant, common-type pumices.

Plagioclase from Lavas I varies from andesine to labradorite ($An_{64-26}$), exceptionally bytownite ($An_{74}$). Zoning is mostly toward An decrease from core to rim, although one analyzed crystal has $An_{39}$ core then jumps to $An_{76}$ and finally yields $An_{38}$ to the rims; this could reflect corrosion in some part of the crystal growth history due to magma chamber recharge (Fig. 8). Plagioclase from Lavas II ranges from andesine to labradorite ($An_{62-33}$) with both direct and reverse zoning.

### 4.5. Fe–Ti oxides

Spinel-group minerals are abundant both as inclusions in clinopyroxene, plagioclase, titanite and biotite, and as a matrix constituent. Representative analyses are given in Table 5. Ilmenite was not found during petrography and microprobe work.

The Fe–Ti oxides analyzed belong to the magnetite-ulvospinel series, with small amounts of MgO (up to 1.5 wt.%, rarely 2.43 wt.%), $Al_2O_3$ (up to 3.1 wt.%, exceptionally 6.53 wt.%), $V_2O_3$ (up to 0.64 wt.%), and very low $Cr_2O_3$ (<0.1 wt.%). $TiO_2$, on the other hand, varies widely (generally up to 13.11 wt.%, and exceptionally up to 25.6 wt.%). In most cases the highest $TiO_2$ (wt.%) content in spinels from a single sample or unit are from spinel inclusions in mafic minerals. The large majority of the analyzed crystals contain over 3 wt.% $TiO_2$, and are therefore classified as Ti-magnetite. Increasing $TiO_2$ (wt.%) contents in titanomagnetite are generally correlated with increasing temperature (e.g., Devine et al., 2003), whereas other oxides, such as MgO and $Al_2O_3$ may be strongly influenced by co-precipitating phases, such as mafic minerals and plagioclase (e.g., Tomiya and Takahashi, 2005).

The ranges of spinel composition from the various units overlap, but those from Arremo ($Usp_{34-2}$) and Lavas I ($Usp_{76-1}$) are much wider than those from Hualfin ($Usp_{19-14}$) and Jasimaná ($Usp_{21-3}$). A single grain analyzed from Alto de Las Lagunas yielded $Usp_8$, and one from the Lavas II Unit yielded $Usp_{10}$. The wider range observed in Arremo and Lavas I in individual magma batches is consistent with magma mixing or thermal/compositional zonation in the chamber (c.f., Tomiya and Takahashi, 2005).

## 5. Whole-rock chemistry

Major and minor elements were determined by XRF at the Universidad Nacional de Salta, rare earth elements and other minor and trace elements were analyzed at the ACME laboratories (Canada) by ICP-MS. Isotopic ratios were determined at the Geochronology Laboratory of the Universidade de Brasília. Analytical methodology is explained in Appendix A.

Absolute values of major, minor and rare earth elements and isotopic ratios are given in Table 6. The ignimbrites composition (on a volatile free basis) is restricted to calc-alkaline dacites and trachydacites (Fig. 9) whereas Lavas I are trachyandesites and minor trachydacites and Lavas II dacites (see Fig. 9). The ignimbrites classify as metaluminous to mildly peraluminous (A/CNK>1), with values ranging from 0.92 to 1.1, their alkalis content is high ($K_2O+Na_2O>6\%$) as it is seen in most of the ignimbrites from the CVZ; both groups of lavas are metaluminous. Correlation diagrams (Fig. 10) for some major and minor elements show tendencies compatible with fractionation of different mineral phases as evidenced by CaO vs $Al_2O_3$

**Table 4**
Representative microprobe analyses of feldspars.

| Unit | Alto de Las Lagunas Ignimbrite | | | | Pucarilla Ignimbrite | | | | | | | | | | | | |
|---|---|---|---|---|---|---|---|---|---|---|---|---|---|---|---|---|---|
| | | | | | Accidental lithic in Hualfín Unit | | Hualfín Unit | | | | | Arremo Unit | | | | | |
| Analysis | CMS-38-4-1 | CMS-38-4-2 | CG4-1-2 | CG4-1-3 | H006B-1-2 | H006B-1-3 | H006B-3-1 | H006B-3-3 | P007-1-1 | P007-1-2 | P007-1-3 | N02-4-1 | N02-4-2 | N02-4-2.5 | N02-4-3.5 | N02-4-4 | N02-4-5 |
| Profile | 66.1 | 66.2 | 60.2 | 60.3 | 92.1 | 92.2 | 94.1 | 94.3 | 89.1 | 89.2 | 89.3 | 46.1 | 46.2 | 46.3 | 46.4 | 46.5 | 46.6 |
| | Pumice | Pumice | Gcm[1] | Gcm[1] | Gcm[1] | Gcm[1] | Pumice | Pumice | Pumice | Pumice | Pumice | Pumice | Pumice | Pumice | Pumice | Pumice | Pumice |
| Position | Rim | Core | Core | Rim | Core | Rim | Rim | Core | Rim | Core | Rim | Rim | | | | | Rim |
| $SiO_2$ | 57.76 | 59.70 | 57.90 | 57.31 | 57.12 | 53.97 | 57.42 | 57.14 | 58.14 | 58.56 | 57.79 | 58.02 | 47.16 | 59.36 | 58.23 | 51.78 | 57.78 |
| $Al_2O_3$ | 26.20 | 25.01 | 25.64 | 25.84 | 26.31 | 28.60 | 25.76 | 25.94 | 25.45 | 25.85 | 25.08 | 25.95 | 32.90 | 25.51 | 26.34 | 29.38 | 26.28 |
| FeO | 0.20 | 0.27 | 0.23 | 0.23 | 0.46 | 0.37 | 0.22 | 0.22 | 0.24 | 0.21 | 0.25 | 0.26 | 0.36 | 0.24 | 0.23 | 0.30 | 0.31 |
| CaO | 8.43 | 7.27 | 7.83 | 8.40 | 8.79 | 11.31 | 8.23 | 8.60 | 8.01 | 8.06 | 7.52 | 8.26 | 16.37 | 7.76 | 8.50 | 12.83 | 8.50 |
| $Na_2O$ | 6.78 | 8.41 | 7.40 | 7.18 | 6.16 | 5.38 | 6.62 | 6.49 | 6.69 | 7.01 | 7.91 | 7.26 | 2.77 | 6.21 | 6.27 | 4.24 | 7.25 |
| $K_2O$ | 0.52 | 0.73 | 0.68 | 0.67 | 0.65 | 0.36 | 0.72 | 0.62 | 0.82 | 0.83 | 0.83 | 0.68 | 0.13 | 0.79 | 0.69 | 0.28 | 0.67 |
| BaO | 0.06 | 0.04 | 0.00 | 0.00 | 0.00 | 0.09 | 0.00 | 0.09 | 0.00 | 0.10 | 0.03 | 0.01 | 0.00 | 0.00 | 0.00 | 0.15 | 0.09 |
| SrO | 0.00 | 0.00 | 0.00 | 0.02 | 0.16 | 0.00 | 0.00 | 0.02 | 0.05 | 0.10 | 0.07 | 0.01 | 0.25 | 0.03 | 0.00 | 0.00 | 0.13 |
| Total | 99.93 | 101.42 | 99.68 | 99.64 | 99.65 | 100.08 | 98.96 | 99.13 | 99.38 | 100.72 | 99.48 | 100.44 | 99.92 | 99.90 | 100.26 | 98.96 | 101.00 |

| Unit | Jasimaná Unit–Pucarilla Ignimbrite | | | | | | Lavas I | | | | | | Lavas II | | | | | |
|---|---|---|---|---|---|---|---|---|---|---|---|---|---|---|---|---|---|---|
| Analysis | PAMP01-1-1 | PAMP01-1-2 | PAMP01-1-3 | P002B-1-7 | P002B-1-8 | P002B-1-9 | CMS-18-2-1 | CMS-18-2-2 | CMS-18-2-3 | CMS-18-2-4 | CMS-18-2-5 | CMS-18-2-6 | CMS-30-5-4 | CMS-30-5-5 | CMS-30-5-6 | CMS-30-5-1 | CMS-30-5-2 | CMS-30-5-4A |
| Profile | 56.1 | 56.2 | 56.3 | 54.1 | 54.2 | 54.3 | 68.1 | 68.2 | 68.3 | 68.4 | 68.5 | 68.6 | 75.1 | 75.2 | 75.3 | 74.1 | 74.2 | 74.4 |
| | Pumice | Pumice | Pumice | Pinkp[2] | Pinkp[2] | Pinkp[2] | | | | | | | | | | | | |
| Position | Rim | Core | Rim | Rim | Core | Rim | Rim | | | Core | | Rim | Rim | Core | Rim | Rim | Core | Rim |
| $SiO_2$ | 57.76 | 58.73 | 58.61 | 57.85 | 57.77 | 58.29 | 57.16 | 55.46 | 55.46 | 58.66 | 53.83 | 56.71 | 58.98 | 55.25 | 58.32 | 52.39 | 57.77 | 52.14 |
| $Al_2O_3$ | 25.72 | 24.98 | 25.83 | 26.38 | 27.15 | 26.47 | 26.00 | 27.53 | 26.53 | 25.26 | 28.19 | 26.58 | 25.68 | 27.21 | 26.09 | 29.65 | 26.24 | 29.63 |
| FeO | 0.27 | 0.25 | 0.24 | 0.28 | 0.25 | 0.24 | 0.53 | 0.39 | 0.46 | 0.44 | 0.44 | 0.49 | 0.30 | 0.21 | 0.30 | 0.85 | 0.29 | 0.62 |
| CaO | 8.03 | 6.99 | 7.87 | 8.54 | 9.06 | 8.42 | 8.79 | 10.41 | 9.69 | 7.74 | 11.01 | 9.37 | 7.85 | 10.21 | 8.30 | 12.79 | 8.41 | 13.08 |
| $Na_2O$ | 7.55 | 8.33 | 6.83 | 6.69 | 6.09 | 6.99 | 5.84 | 5.24 | 4.91 | 6.73 | 4.21 | 5.38 | 7.08 | 4.96 | 6.88 | 4.48 | 7.09 | 4.26 |
| $K_2O$ | 0.61 | 0.87 | 0.74 | 0.39 | 0.61 | 0.68 | 0.99 | 0.80 | 0.91 | 1.22 | 0.77 | 1.02 | 0.87 | 0.47 | 0.85 | 0.28 | 0.64 | 0.32 |
| BaO | 0.07 | 0.13 | 0.00 | 0.00 | 0.00 | 0.00 | 0.07 | 0.13 | 0.01 | 0.03 | 0.12 | 0.04 | 0.04 | 0.03 | 0.08 | 0.00 | 0.15 | 0.13 |
| SrO | 0.00 | 0.00 | 0.19 | 0.11 | 0.03 | 0.16 | 0.15 | 0.01 | 0.16 | 0.12 | 0.12 | 0.00 | 0.03 | 0.02 | 0.09 | 0.00 | 0.00 | 0.09 |
| Total | 100.00 | 100.26 | 100.30 | 100.22 | 100.97 | 101.25 | 99.52 | 99.96 | 98.14 | 100.19 | 98.69 | 99.59 | 100.82 | 98.35 | 100.91 | 100.45 | 100.59 | 100.27 |

[1]Grey crystal mush. [2]pink pumice.

**Table 5**
Representative microprobe analyses of spinels.

| Unit | Pucarilla Ignimbrite | | | | | | | | | | Lavas I | | Lavas II |
|---|---|---|---|---|---|---|---|---|---|---|---|---|---|
| | Hualfín Unit | | | Arremo Unit | | | | Jasimaná Unit | | | | | |
| Analysis | D-02-10-A1 | D-02-7B-2 | D-02-4B-4 | PAMP-02-3B-1 | PAMP-02-3B-2 | PAMP-02-3A-2 | PAMP-02-3B-1 | P002B-3C-1 | D-04-2A-1 | D-04-2A-3 | SCMS-21-1-C2A | SCMS-21-3C1 | SCMS-30-2-C1 |
| | Pumice | Pumice | | Pumice | | | Pumice | Pumice | Pumice | | | | |
| Position | Core | Core | Core | Core | Core | Rim | Core | Core | Core | | Rim | Core | Core |
| $SiO_2$ | 0.06 | 0.06 | 0.10 | 0.00 | 0.09 | 0.05 | 0.00 | 0.00 | 0.03 | 0.00 | 0.11 | 0.63 | 0.11 |
| $Al_2O_3$ | 1.16 | 2.48 | 2.16 | 1.34 | 1.26 | 1.49 | 1.34 | 1.23 | 2.07 | 1.02 | 2.14 | 2.19 | 1.31 |
| $TiO_2$ | 4.64 | 5.11 | 2.91 | 2.30 | 2.59 | 2.65 | 2.30 | 0.92 | 2.57 | 3.56 | 7.73 | 7.28 | 3.32 |
| FeO | 33.31 | 33.40 | 31.61 | 31.44 | 32.19 | 31.47 | 31.44 | 27.25 | 31.26 | 32.23 | 37.03 | 36.02 | 32.00 |
| MnO | 1.23 | 1.14 | 1.07 | 0.57 | 0.54 | 0.76 | 0.57 | 0.84 | 0.71 | 0.84 | 0.40 | 0.61 | 0.72 |
| MgO | 0.54 | 0.89 | 0.69 | 0.70 | 0.56 | 0.73 | 0.70 | 2.43 | 0.98 | 0.67 | 0.59 | 1.07 | 1.04 |
| CaO | 0.01 | 0.03 | 0.14 | 0.02 | 0.00 | 0.01 | 0.02 | 0.00 | 0.02 | 0.14 | 0.09 | 0.05 | 0.13 |
| $Cr_2O_3$ | 0.07 | 0.06 | 0.05 | 0.04 | 0.10 | 0.06 | 0.04 | 0.09 | 0.07 | 0.01 | 0.09 | 0.03 | 0.08 |
| $Fe_2O_3$ | 57.99 | 56.02 | 60.26 | 62.56 | 62.05 | 61.38 | 62.56 | 66.12 | 61.16 | 60.60 | 50.43 | 49.73 | 61.10 |
| ZnO | 0.03 | 0.32 | 0.21 | 0.16 | 0.12 | 0.15 | 0.16 | 0.10 | 0.06 | 0.08 | 0.01 | 0.14 | 0.12 |
| $V_2O_3$ | 0.26 | 0.32 | 0.32 | 0.39 | 0.24 | 0.26 | 0.39 | 0.43 | 0.22 | 0.26 | 0.41 | 0.40 | 0.30 |
| NiO | 0.00 | 0.00 | 0.00 | 0.00 | 0.00 | 0.08 | 0.00 | 0.10 | 0.00 | 0.00 | 0.10 | 0.00 | 0.04 |
| Total | 99.29 | 99.83 | 99.52 | 99.52 | 99.74 | 99.08 | 99.52 | 99.51 | 99.15 | 99.39 | 99.13 | 98.15 | 100.26 |

(plagioclase), MgO vs CaO (pyroxene), $P_2O_5$ vs $SiO_2$ (apatite), $SiO_2$ vs MgO (pyroxene), $SiO_2$ vs Sr (plagioclase) and also versus other trace elements (diagrams not shown) as Ba (biotite) and Y (amphibole).

Absolute $SiO_2$ (wt.%) is between 60.9 and 66.6, the most silicic units being the Alto de Las Lagunas and Luingo I and Luingo II Ignimbrites. Mg# is between 0.32 and 0.5 for the pyroclastic facies,

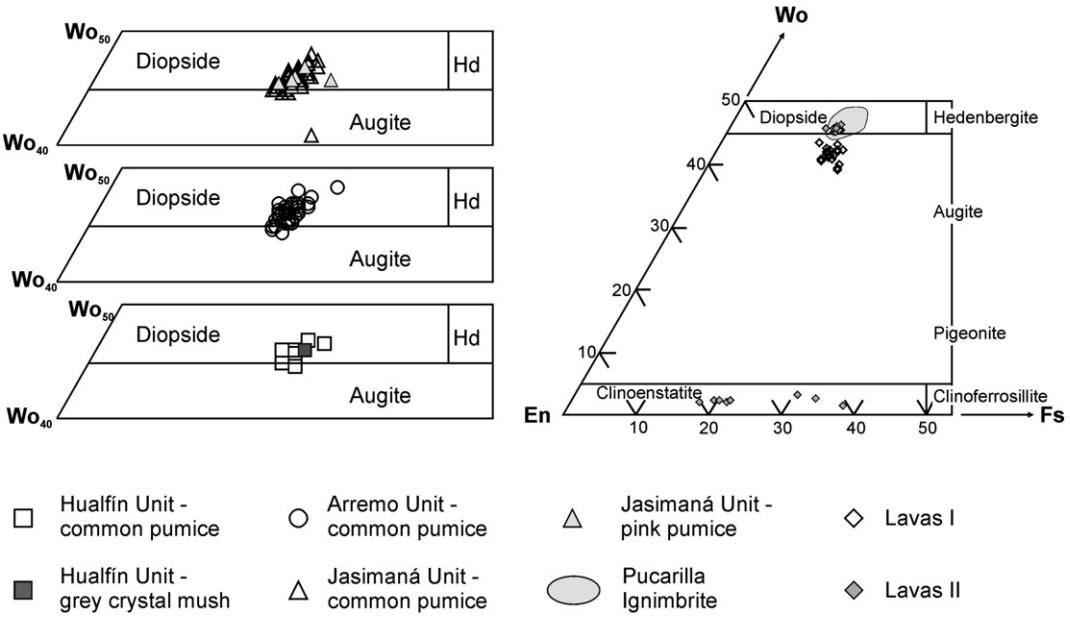


**Fig. 4.** Pyroxenes from Luingo caldera pumices plotted in the Morimoto (1988) classification diagram.

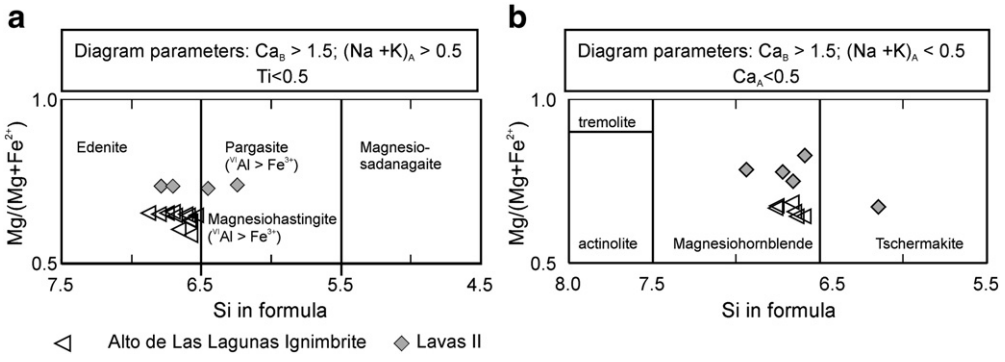


**Fig. 5.** Calcic amphiboles from the PCTVC classified in the Leake et al. (1997) diagrams.

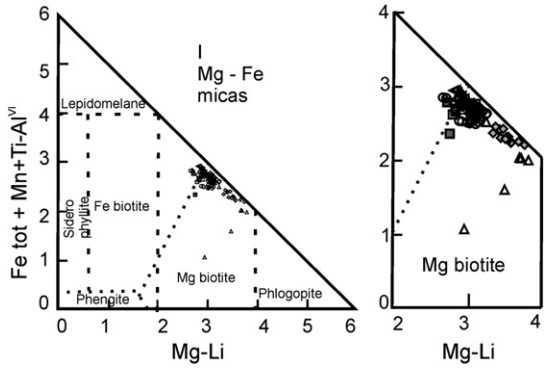


**Fig. 6.** Micas from PCTVC plotted in the Tischendorf (1997) classification diagram. Symbols as in Figs. 4 and 5.

and is highest in the Hualfin Unit, intermediate in the Arremo Unit and the lowest in the Jasimaná Unit and Alto de Las Lagunas Ignimbrite. In some cases there is a marked variation in the absolute content of major elements even within samples of a given unit. This is particularly evident in the Jasimaná Unit where $SiO_2$ (wt.%) can vary by ~3–4%; variations are also recorded in minor elements both mobile and immobile (e.g., Ba, Rb, Sr, Zr, and Y) but is sharper in the first ones. In the Pucarilla Ignimbrite – where more samples were collected and analyzed – compositional variations within units are evident from vertical profiles. These are especially obvious for $SiO_2$, $K_2O$ and Rb, which are higher in the central parts of each unit (Fig. 11). The pattern displayed by $K_2O$ (wt.%) fits well with classical devitrification patterns in ignimbrites (Smith, 1960), where the more devitrified zones (enrichment in $K_2O$: e.g., Lipman, 1965; Kochhar, 1977) are in the middle sectors. We interpret that, at least in the case of $SiO_2$ and of mobile elements, these variations might be related to post-depositional processes like vapour-phase alteration. In the case of immobile elements such as Zr and Y, this variation within each ignimbrite could be better

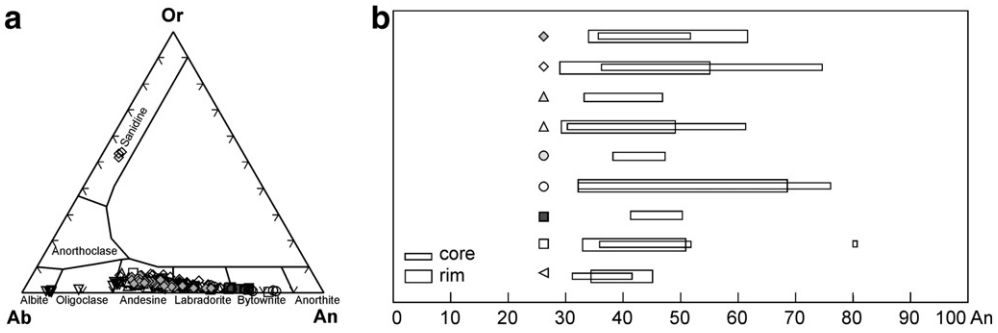


**Fig. 7.** Feldspars from PCTVC a) An–Or–Ab classification diagram, b) anorthite range content for plagioclases of the different units of PCTVC. Down-pointing triangles belong to Luingo II Ignimbrite, light-grey circles are from Arremo Unit pink pumices and other symbols as in the figures above.

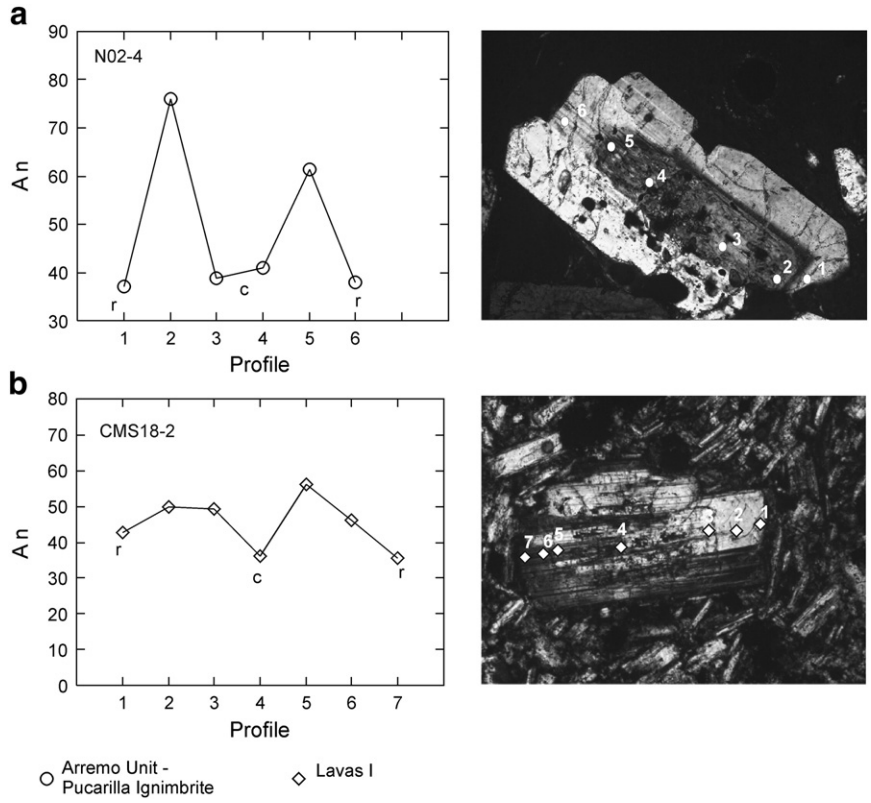


**Fig. 8.** Selected plagioclase profiles a) Arremo Unit–Pucarilla Ignimbrite; b) Lavas I.

**Table 6**
Geochemical analyses showing absolute values of major, minor and rare earth elements and isotopic ratios.

| Unit | Luingo I Ignimbrite | | Luingo II Ignimbrite | | | Alto de Las Lagunas Ignimbrite | | | Hualfín Unit–Pucarilla Ignimbrite | | | | |
|---|---|---|---|---|---|---|---|---|---|---|---|---|---|
| Sample | CMS-05 | CMS-07 | PAMP04 | CMS-13 | CMS-15 | CMS-38 | CMS-38PR | CG-04 | D-02 | H-006 | H-008 | P-007 | PAMP06 |
| Location | 26 07 39.1 S 66 34 53.6 W | 26 07 38 S 66 34 55.1 W | 26 05 44.2 S 66 33 0.1 W | 26 07 38 S 66 34 55.1 W | 26 08 16.4 S 66 36 08.3 W | 26 05 13.7 S 66 41 15.7 W | 26 05 13.7 S 66 41 15.7 W | 25 59 50 S 66 45 24.9 W | 25 56 20.7 S 66 19 27.1 W | 25 48 59.6 S 66 21 50.1 W | 25 48 59.6 S 66 21 50.1 W | 25 56 9.7 S 66 17 47.6 W | 25 56 09.3 S 66 17 50.7 W |
| $SiO_2$ | 66.44 | 65.48 | 63.87 | 61.26 | 62.77 | 65.03 | 66.61 | 65.61 | 60.91 | 61.96 | 62.07 | 65.14 | 65.13 |
| $Al_2O_3$ | 15.88 | 15 | 15.84 | 15.67 | 14.62 | 15.7 | 15.68 | 15.5 | 16.45 | 15.78 | 16.01 | 14.35 | 15.05 |
| $Fe_2O_3$ | 2.93 | 3.44 | 4.66 | 4.94 | 4.07 | 4.96 | 3.7 | 3.65 | 4.99 | 4.58 | 4.65 | 4.36 | 4.1 |
| MnO | 0.05 | 0.09 | 0.1 | 0.1 | 0.1 | 0.13 | 0.03 | 0.05 | 0.11 | 0.11 | 0.1 | 0.09 | 0.09 |
| MgO | 1.2 | 1.66 | 2.02 | 2.18 | 1.61 | 1.23 | 1.14 | 1.16 | 2.28 | 2.38 | 2.4 | 1.8 | 1.68 |
| CaO | 2.54 | 3.28 | 3.93 | 4.47 | 4.49 | 3.4 | 3 | 3.47 | 4.29 | 3.37 | 3.4 | 3 | 3.17 |
| $Na_2O$ | 2.37 | 2.7 | 3.06 | 2.64 | 2.14 | 2.77 | 2.58 | 3.13 | 2.93 | 2.73 | 2.61 | 2.76 | 2.93 |
| $K_2O$ | 5.8 | 4.41 | 4.18 | 4.24 | 4.35 | 4.19 | 4.35 | 4.27 | 3.65 | 3.73 | 3.62 | 4.36 | 4.15 |
| $P_2O_5$ | 0.23 | 0.24 | 0.26 | 0.32 | 0.26 | 0.26 | 0.22 | 0.24 | 0.28 | 0.27 | 0.28 | 0.27 | 0.26 |
| $TiO_2$ | 0.44 | 0.47 | 0.63 | 0.67 | 0.54 | 0.62 | 0.5 | 0.68 | 0.67 | 0.66 | 0.63 | 0.63 | 0.58 |
| LOI | 2 | 3.02 | 1.97 | 3.73 | 5.54 | 1.71 | 2.35 | 1.29 | 3.22 | 3.77 | 3.94 | 2.8 | 2.98 |
| Total | 99.88 | 99.79 | 100.52 | 100.22 | 100.49 | 100 | 100.16 | 99.05 | 99.78 | 99.34 | 99.71 | 99.56 | 100.12 |
| Cr | 7 | 4 | 7 | 12 | 2 | 5 | 4 | | 5 | 8 | 8 | 7 | 7 |
| Ba | 588 | 563 | 602 | 593 | 619 | 402 | 397 | | 553 | 491 | 491 | 403 | 491 |
| Be | 2 | 3 | 3 | 1 | 1 | 2 | 3 | | 3 | 3 | 2 | 3 | 3 |
| Cs | 6.3 | 9 | 5.9 | 14.2 | 5.9 | 7.1 | 8.3 | | 6.3 | 8.8 | 8.4 | 11.5 | 11.5 |
| Ga | 17.9 | 17 | 18.6 | 19 | 17.2 | 17.2 | 17.5 | | 19.1 | 19.6 | 19.6 | 16.8 | 19.5 |
| Hf | 4.7 | 4.9 | 5.7 | 5 | 4.7 | 4.7 | 5.3 | | 6 | 6.6 | 6 | 5.3 | 5.1 |
| Nb | 23.2 | 21.4 | 23.3 | 25.2 | 22.4 | 22.3 | 21.7 | | 23.2 | 26.7 | 26.4 | 26.8 | 25 |
| Rb | 237 | 180 | 169 | 179 | 184 | 177 | 186 | | 145 | 168 | 168 | 200 | 195 |
| Sn | 2 | 2 | 2 | 2 | 1 | 2 | 2 | | 2 | 2 | 3 | 2 | 2 |
| Sr | 409 | 469 | 492 | 485 | 410 | 379 | 366 | | 508 | 428 | 433 | 355 | 409 |
| Ta | 1.6 | 1.4 | 1.7 | 1.7 | 1.5 | 1.6 | 1.6 | | 1.6 | 2 | 1.9 | 2 | 1.9 |
| Th | 21.6 | 19.4 | 17.5 | 14.6 | 17.3 | 16.5 | 19.5 | | 15.9 | 24.3 | 23.2 | 24.7 | 22.6 |
| U | 5.3 | 4.9 | 4.4 | 3.9 | 3.9 | 3.8 | 4 | | 4 | 4.5 | 4.2 | 5.3 | 4.9 |
| V | 63 | 66 | 95 | 99 | 70 | 103 | 88 | | 98 | 91 | 91 | 86 | 89 |
| Zr | 177 | 189 | 190 | 195 | 184 | 173 | 202 | | 229 | 230 | 228 | 180 | 180 |
| Y | 21.6 | 21.2 | 24.3 | 25.5 | 24.5 | 36.2 | 27.1 | | 23.1 | 25.4 | 23.9 | 26.1 | 23.8 |
| La | 41.6 | 37.4 | 40.6 | 39.5 | 37.8 | 33.2 | 35.2 | | 38.5 | 45.5 | 44.3 | 43.5 | 43.2 |
| Ce | 81.3 | 72.8 | 87.5 | 83.9 | 78.1 | 73.3 | 70.1 | | 82.3 | 94.4 | 91.7 | 96.6 | 88 |
| Pr | 8.1 | 7.33 | 9.01 | 9.15 | 8.17 | 8.53 | 8.24 | | 9.19 | 9.5 | 9.55 | 9.6 | 8.76 |
| Nd | 27.6 | 25.5 | 30.7 | 32 | 29.4 | 31.6 | 29.5 | | 30.9 | 36.7 | 31.6 | 34.9 | 31.9 |
| Sm | 4.91 | 4.42 | 6.4 | 6.15 | 5.51 | 6.46 | 5.79 | | 6.4 | 6.1 | 6 | 7.5 | 6 |
| Eu | 1.1 | 0.96 | 1.04 | 1.32 | 1.13 | 1.24 | 1.12 | | 1.09 | 1.18 | 1.11 | 1.07 | 1.07 |
| Gd | 3.63 | 3.49 | 4.1 | 4.77 | 4.25 | 5.61 | 4.72 | | 4.4 | 3.85 | 3.99 | 5.08 | 4.81 |
| Tb | 0.61 | 0.58 | 0.65 | 0.78 | 0.72 | 0.98 | 0.82 | | 0.77 | 0.9 | 0.73 | 0.94 | 0.67 |
| Dy | 2.88 | 2.85 | 3.54 | 3.63 | 3.36 | 4.95 | 3.88 | | 3.88 | 4.09 | 3.34 | 3.73 | 3.9 |
| Ho | 0.56 | 0.54 | 0.76 | 0.72 | 0.68 | 0.93 | 0.73 | | 0.72 | 0.82 | 0.71 | 0.86 | 0.82 |
| Er | 1.81 | 1.81 | 2.21 | 2.18 | 2.15 | 3.11 | 2.32 | | 2.15 | 2.22 | 2.27 | 2.42 | 2.03 |
| Tm | 0.27 | 0.25 | 0.35 | 0.32 | 0.32 | 0.44 | 0.35 | | 0.35 | 0.37 | 0.39 | 0.39 | 0.35 |
| Yb | 2 | 1.88 | 2.44 | 2.17 | 2.19 | 3.09 | 2.43 | | 1.78 | 2.37 | 2.1 | 2.44 | 2.29 |
| Lu | 0.31 | 0.3 | 0.29 | 0.31 | 0.3 | 0.46 | 0.37 | | 0.4 | 0.42 | 0.43 | 0.36 | 0.36 |
| $^{143}Nd/^{144}$\Ndm | | | | | | 0.512321 ± 12 | | 0.512308 ± 13 | 0.512441 ± 5 | | 0.512375 ± 7 | 0.512411 ± 5 | 0.512384 ± 16 |
| $^{143}Nd/^{144}Ndi$ | | | | | | 0.512311 | | 0.512298 | 0.512432 | | 0.512367 | 0.512402 | 0.512375 |
| $^{147}Sm/^{144}Nd$ | | | | | | 0.1156 | | 0.1131 | 0.11 | | 0.1065 | 0.1091 | 0.1106 |
| εNd (t) | | | | | | −6.05 | | −6.30 | −3.71 | | −4.99 | −4.29 | −4.82 |
| TDM | | | | | | 1.12 | | 1.11 | 0.90 | | 0.95 | 0.10 | 0.97 |
| $^{87}Sr/^{86}Srm$ | | | | | | 0.70877 ± 2 | | 0.70871 ± 2 | 0.70809 ± 3 | | 0.70937 ± 33 | 0.70778 ± 2 | 0.70928 ± 3 |
| $^{87}Sr/^{86}Sri$ | | | | | | 0.70852 | | | 0.70795 | | 0.70918 | 0.70777 | 0.70904 |

| Unit | Arremo Unit–Pucarilla Ignimbrite | | | | | | Jasimaná Unit–Pucarilla Ignimbrite | | | | | | | |
|---|---|---|---|---|---|---|---|---|---|---|---|---|---|---|
| Sample | D-03 | PAMP02 | D-07 | N-02 | P-008 | PAMP09 | D-04 | D-08 | CMS-31 | H-009 | P-002 | P-006 | PAMP01 | CG-01 |
| Location | 25 56 20.7 S 66 19 27.1 W | 26 09 43.7 S 66 27 50.9 W | 25 58 11.9 S 66 18 41.8 W | 25 56 9.4 S 66 17 50.9 W | 25 56 9.7 S 66 17 47.6 W | 25 56 09.3 S 66 17 50.7 W | 25 56 20.7 S 66 19 27.1 W | 25 58 11.9 S 66 18 41.8 W | 26 09 22.6 S 66 44 51.8 W | 25 48 59.6 S 66 21 50.1 W | 25 54 31.1 S 66 19 29.4 W | 25 55 18.7 S 66 19 15 W | 26 09 30.6 S 66 27 47.7 W | 25 56 27 S 66 38 10.9 W |
| $SiO_2$ | 61.73 | 62.51 | 63.21 | 65.24 | 64.86 | 64.64 | 62.81 | 62.39 | 63.63 | 65.54 | 64 | 63.97 | 63.65 | 64.87 |
| $Al_2O_3$ | 16.47 | 16.52 | 15.1 | 14.72 | 14.87 | 14.56 | 16.67 | 16.59 | 16.4 | 16.13 | 15.93 | 15.89 | 16.45 | 15.85 |
| $Fe_2O_3$ | 4.9 | 4.95 | 4.59 | 4.25 | 4.41 | 4.08 | 5.18 | 5.06 | 4.83 | 4.28 | 4.66 | 4.57 | 4.97 | 4.25 |
| MnO | 0.1 | 0.11 | 0.1 | 0.1 | 0.1 | 0.09 | 0.1 | 0.11 | 0.1 | 0.1 | 0.1 | 0.11 | 0.11 | 0.1 |
| MgO | 2.1 | 2.03 | 2.01 | 1.8 | 1.91 | 1.76 | 1.98 | 1.72 | 1.47 | 1.1 | 1.7 | 1.57 | 1.84 | 1.6 |
| CaO | 4.37 | 4.64 | 3.71 | 3.28 | 3.56 | 3.48 | 4.52 | 4.25 | 4.01 | 3.69 | 4.04 | 4.1 | 4.52 | 3.82 |
| $Na_2O$ | 3.12 | 3.24 | 2.93 | 2.87 | 2.96 | 2.96 | 3.32 | 3.41 | 3.3 | 3.19 | 3.3 | 3.09 | 3.26 | 3.34 |
| $K_2O$ | 3.3 | 3.9 | 4.08 | 4.43 | 4.38 | 4.44 | 3.92 | 3.91 | 4.31 | 4.46 | 4.19 | 4.29 | 4.06 | 4.3 |
| $P_2O_5$ | 0.28 | 0.27 | 0.27 | 0.26 | 0.27 | 0.25 | 0.31 | 0.28 | 0.29 | 0.26 | 0.29 | 0.27 | 0.28 | 0.26 |
| $TiO_2$ | 0.66 | 0.66 | 0.63 | 0.59 | 0.61 | 0.59 | 0.69 | 0.7 | 0.66 | 0.59 | 0.64 | 0.63 | 0.66 | 0.59 |

(continued on next page)

**Table 6** (*continued*)

| Unit | Arremo Unit–Pucarilla Ignimbrite | | | | | | Jasimaná Unit–Pucarilla Ignimbrite | | | | | | | |
|---|---|---|---|---|---|---|---|---|---|---|---|---|---|---|
| Sample | D-03 | PAMP02 | D-07 | N-02 | P-008 | PAMP09 | D-04 | D-08 | CMS-31 | H-009 | P-002 | P-006 | PAMP01 | CG-01 |
| Location | 25 56 20.7 S 66 19 27.1 W | 26 09 43.7 S 66 27 50.9 W | 25 58 11.9 S 66 18 41.8 W | 25 56 9.4 S 66 17 50.9 W | 25 56 9.7 S 66 17 47.6 W | 25 56 09.3 S 66 17 50.7 W | 25 56 20.7 S 66 19 27.1 W | 25 58 11.9 S 66 18 41.8 W | 26 09 22.6 S 66 44 51.8 W | 25 48 59.6 S 66 21 50.1 W | 25 54 31.1 S 66 19 29.4 W | 25 55 18.7 S 66 19 15 W | 26 09 30.6 S 66 27 47.7 W | 25 56 27 S 66 38 10.9 W |
| LOI | 2.33 | 1.38 | 3.22 | 2.52 | 2.33 | 2.48 | 0.63 | 0.77 | 0.82 | 1.18 | 0.55 | 1.25 | 0.7 | 0.38 |
| Total | 99.36 | 100.21 | 99.85 | 100.06 | 100.26 | 99.18 | 100.13 | 99.19 | 99.82 | 100.52 | 99.4 | 99.74 | 100.5 | 99.36 |
| Cr | 19 | 8 | 8 | 5 | 6 | 11 | 8 | 10 | 7 | 6 | 11 | 5 | 7 | |
| Ba | 540 | 549 | 476 | 470 | 504 | 496 | 560 | 569 | 654 | 627 | 569 | 556 | 555 | |
| Be | 3 | 3 | 3 | 3 | 3 | 3 | 3 | 3 | 2 | 2 | 3 | 3 | 3 | |
| Cs | 7.9 | 9.3 | 13.6 | 13 | 11.1 | 11.6 | 6.5 | 5.6 | 6.6 | 6.2 | 8.3 | 7.4 | 6.1 | |
| Ga | 20.2 | 20.8 | 20.2 | 17.9 | 16.1 | 17.25 | 22.2 | 20.7 | 19.4 | 19.3 | 20.5 | 18.2 | 20.6 | |
| Hf | 5.2 | 5.9 | 5.7 | 5.9 | 5.3 | 5.7 | 4.7 | 5.3 | 5.4 | 5.5 | 6.2 | 5.5 | 6.1 | |
| Nb | 24.9 | 25.9 | 25.7 | 24.5 | 24.9 | 24.7 | 25.7 | 25.4 | 25.3 | 23 | 24.8 | 24.6 | 23.7 | |
| Rb | 161 | 167 | 180 | 191 | 194 | 193 | 157 | 145 | 175 | 182 | 178 | 179 | 165 | |
| Sn | 2 | 2 | 2 | 2 | 2 | 2 | 2 | 2 | 1 | 2 | 2 | 2 | 2 | |
| Sr | 527 | 562 | 407 | 387 | 418 | 402 | 540 | 525 | 550 | 465 | 496 | 500 | 527 | |
| Ta | 1.7 | 1.8 | 1.9 | 1.7 | 1.9 | 1.95 | 1.7 | 1.7 | 1.7 | 1.8 | 1.9 | 1.9 | 1.9 | |
| Th | 17.5 | 20.6 | 19.1 | 18.7 | 21.7 | 21.3 | 16.2 | 15 | 19 | 19.6 | 19 | 18.7 | 16.8 | |
| U | 4.1 | 4.2 | 4.5 | 5.2 | 5.3 | 5.35 | 4 | 3.8 | 3.6 | 4.3 | 4.1 | 4 | 3.8 | |
| V | 99 | 112 | 88 | 90 | 97 | 88.5 | 108 | 102 | 85 | 84 | 84 | 104 | 99 | |
| Zr | 196 | 198 | 194 | 197 | 182 | 173 | 196 | 196 | 205 | 204 | 192 | 184 | 203 | |
| Y | 25.8 | 27.8 | 25.5 | 22.5 | 25.4 | 24 | 27.1 | 24.7 | 26.3 | 22.2 | 25.3 | 24.2 | 26.4 | |
| La | 43.2 | 43.4 | 43.5 | 41.3 | 42.9 | 42.75 | 43.3 | 42.2 | 41.5 | 42.3 | 42.1 | 42 | 41.5 | |
| Ce | 91.3 | 94.8 | 89.5 | 86.6 | 93.6 | 90.1 | 92.3 | 89.1 | 89.2 | 82.5 | 90.2 | 86.8 | 88.1 | |
| Pr | 9.47 | 9.64 | 9.27 | 8.66 | 9.15 | 9.17 | 9.55 | 9.5 | 9.7 | 8.68 | 9.01 | 9.13 | 9.66 | |
| Nd | 38 | 36.1 | 34.3 | 28.7 | 32.3 | 32.25 | 34.8 | 37.5 | 35.5 | 30.2 | 32.1 | 33.4 | 37.7 | |
| Sm | 6.3 | 6.9 | 6.3 | 5.4 | 6.3 | 6.55 | 6.6 | 6.8 | 6.38 | 6 | 6.4 | 6.1 | 7.2 | |
| Eu | 1.29 | 1.36 | 1.1 | 1.04 | 1.06 | 1.03 | 1.48 | 1.3 | 1.43 | 1.08 | 1.25 | 1.26 | 1.22 | |
| Gd | 4.88 | 4.94 | 4.36 | 4.23 | 3.91 | 4.31 | 4.86 | 3.88 | 5.06 | 3.17 | 4.53 | 4.4 | 4.89 | |
| Tb | 0.8 | 0.8 | 0.81 | 0.78 | 0.89 | 0.75 | 0.88 | 0.84 | 0.86 | 0.74 | 0.82 | 0.73 | 0.87 | |
| Dy | 4.14 | 4.15 | 4.11 | 3.87 | 3.92 | 3.65 | 4.57 | 4.23 | 4 | 3.45 | 4.05 | 3.43 | 3.95 | |
| Ho | 0.81 | 0.99 | 0.76 | 0.75 | 0.87 | 0.76 | 0.82 | 0.72 | 0.74 | 0.68 | 0.83 | 0.77 | 0.82 | |
| Er | 2.15 | 2.56 | 2.24 | 2.21 | 2.2 | 2.26 | 2.44 | 2.05 | 2.33 | 1.96 | 1.98 | 2.14 | 2.26 | |
| Tm | 0.35 | 0.38 | 0.33 | 0.37 | 0.4 | 0.34 | 0.35 | 0.35 | 0.33 | 0.32 | 0.36 | 0.3 | 0.32 | |
| Yb | 2.01 | 2.51 | 2.15 | 2.45 | 2.35 | 2.28 | 2.01 | 1.77 | 2.28 | 1.92 | 2.41 | 2.6 | 2.4 | |
| Lu | 0.41 | 0.38 | 0.4 | 0.32 | 0.4 | 0.36 | 0.44 | 0.39 | 0.32 | 0.34 | 0.36 | 0.33 | 0.4 | |
| $^{143}Nd/^{144}Ndm$ | 0.512355 ± 10 | | | 0.512462 ± 7 | | | | 0.512377 ± 15 | | | 0.512470 ± 10 | | 0.512398 ± 13 | |
| $^{143}Nd/^{144}Ndi$ | 0.512346 | | | 0.512455 | | | | 0.512368 | | | 0.512455 | | 0.512390 | |
| $^{147}Sm/^{144}Nd$ | 0.11 | | | 0.09 | | | | 0.1115 | | | 0.19 | | 0.11 | |
| εNd (t) | −5.39 | | | −3.28 | | | | −4.96 | | | −3.27 | | −4.54 | |
| TDM | 1.02 | | | 0.75 | | | | 0.29 | | | | | 0.91 | |
| $^{87}Sr/^{86}Srm$ | 0.70869 ± 2 | | | 0.70850 ± 2 | | | | 0.70764 ± 2 | | | 0.70776 ± 2 | | 0.70793 ± 3 | |
| $^{87}Sr/^{86}Sri$ | 0.70854 | | | 0.70826 | | | | 0.70750 | | | 0.70758 | | 0.70778 | |

| Unit | Lavas I | | | | | Lavas II | | |
|---|---|---|---|---|---|---|---|---|
| Sample | CMS-18 | CMS-21 | CMS-24A | CMS-42 | CMS-03 | CMS-29A | CMS-28 | CMS-30 |
| Location | 26 08 21.3 S 66 36 13.8 W | 26 08 35.6 S 66 36 24.1 W | 26 07 31.7 S 66 37 23.6 W | 26 06 44.5 S 66 37 40.6 W | 26 07 37.1 S 66 34 38.3 W | 26 06 47 S 66 40 25.7 W | 27 06 47 S 66 40 25.7 W | 26 09 19.1 S 66 42 51.5 W |
| $SiO_2$ | 59.68 | 60.87 | | 58.34 | 65.81 | 65.43 | 66.39 | 64.16 |
| $Al_2O_3$ | 16.89 | 16.5 | 15.61 | 15.66 | 15.68 | 15.75 | 15.44 | 15.52 |
| $Fe_2O_3$ | 5.32 | 5.77 | 6.89 | 6.25 | 3.27 | 3.85 | 3.6 | 4.59 |
| MnO | 0.14 | 0.07 | 0.09 | 0.07 | 0.08 | 0.06 | 0.06 | 0.07 |
| MgO | 2.18 | 2.36 | 3.66 | 3.35 | 1.31 | 1.86 | 1.68 | 1.65 |
| CaO | 4.95 | 4.48 | 6.26 | 5.43 | 2.03 | 3.49 | 3.34 | 4.11 |
| $Na_2O$ | 3.19 | 2.66 | 2.82 | 2.92 | 2.83 | 3.25 | 3.38 | 3.03 |
| $K_2O$ | 4.42 | 4.56 | 4.18 | 4.85 | 5.13 | 3.91 | 4.13 | 3.69 |
| $P_2O_5$ | 0.42 | 0.42 | 0.53 | 0.53 | 0.28 | 0.22 | 0.22 | 0.27 |
| $TiO_2$ | 0.7 | 0.69 | 0.87 | 0.81 | 0.57 | 0.54 | 0.52 | 0.62 |
| LOI | 1.38 | 2.08 | 1.79 | 2.04 | 2.09 | 1.89 | 1.57 | 1.67 |
| Total | 99.27 | 100.46 | 42.7 | 100.25 | 99.06 | 100.25 | 100.33 | 99.38 |
| Cr | | | 17 | 35 | | 10 | 12 | 56 |
| Ba | 886 | 919 | 870 | 1127 | 586 | 580 | 555 | 644 |
| Be | 3 | 3 | 2 | 3 | 2 | 2 | 2 | 2 |
| Cs | 5.1 | 2.7 | 3.6 | 3.3 | 7.8 | 14.1 | 11.4 | 39 |
| Ga | 19.7 | 19.2 | 19.9 | 19 | 18.1 | 22.4 | 21.5 | 20.8 |
| Hf | 6.1 | 7.1 | 6.3 | 6.2 | 5.1 | 5.2 | 5 | 5.8 |
| Nb | 25.7 | 25.6 | 25.7 | 26.3 | 24.2 | 15.1 | 14.6 | 14.8 |
| Rb | 162 | 204 | 169 | 203 | 223.7 | 191 | 208 | 171 |
| Sn | 2 | 2 | 2 | 2 | 2 | 2 | 2 | 2 |
| Sr | 746 | 554 | 710 | 734 | 368.7 | 402 | 361 | 438 |
| Ta | 1.5 | 1.6 | 1.7 | 1.7 | 1.6 | 1.2 | 1.1 | 1.2 |
| Th | 12.7 | 17.3 | 16.8 | 16.9 | 19 | 30.4 | 28.6 | 22 |
| U | 3.3 | 3.4 | 3.9 | 4.1 | 5.3 | 6.6 | 6.7 | 5.5 |
| V | 102 | 101 | 197 | 168 | 85 | 78 | 73 | 95 |

**Table 6** (*continued*)

| Unit | Lavas I | | | | | Lavas II | | |
|---|---|---|---|---|---|---|---|---|
| Sample | CMS-18 | CMS-21 | CMS-24A | CMS-42 | CMS-03 | CMS-29A | CMS-28 | CMS-30 |
| Location | 26 08 21.3 S 66 36 13.8 W | 26 08 35.6 S 66 36 24.1 W | 26 07 31.7 S 66 37 23.6 W | 26 06 44.5 S 66 37 40.6 W | 26 07 37.1 S 66 34 38.3 W | 26 06 47 S 66 40 25.7 W | 27 06 47 S 66 40 25.7 W | 26 09 19.1 S 66 42 51.5 W |
| Zr | 263 | 262 | 241 | 246 | 194.5 | 195 | 195 | 219 |
| Y | 28.5 | 32.4 | 30.2 | 27.8 | 22.8 | 18.6 | 17 | 24 |
| La | 44.7 | 46.9 | 45.1 | 47 | 42.5 | 45.4 | 43.8 | 45.2 |
| Ce | 98.7 | 101 | 100.2 | 104.8 | 80.6 | 98.3 | 92.9 | 91 |
| Pr | 11.03 | 11.45 | 11.44 | 12.01 | 8.6 | 10.41 | 9.97 | 10.41 |
| Nd | 39.7 | 41.7 | 41.9 | 43.5 | 31.8 | 36.6 | 34.8 | 38.4 |
| Sm | 7.61 | 8.06 | 8.15 | 8.22 | 5.36 | 6.45 | 6.21 | 6.8 |
| Eu | 1.63 | 1.67 | 1.76 | 1.71 | 1.17 | 1.17 | 1.07 | 1.28 |
| Gd | 5.65 | 6.04 | 6.36 | 6.04 | 4.29 | 4.39 | 3.98 | 4.99 |
| Tb | 0.92 | 1.02 | 0.98 | 0.94 | 0.7 | 0.67 | 0.61 | 0.77 |
| Dy | 4.5 | 4.68 | 4.66 | 4.4 | 3.36 | 2.92 | 2.71 | 3.33 |
| Ho | 0.78 | 0.86 | 0.86 | 0.81 | 0.68 | 0.49 | 0.47 | 0.62 |
| Er | 2.41 | 2.78 | 2.54 | 2.4 | 2.15 | 1.47 | 1.31 | 1.78 |
| Tm | 0.33 | 0.39 | 0.36 | 0.34 | 0.34 | 0.21 | 0.17 | 0.25 |
| Yb | 2.34 | 2.76 | 2.39 | 2.33 | 2.23 | 1.43 | 1.31 | 1.71 |
| Lu | 0.34 | 0.4 | 0.34 | 0.33 | 0.33 | 0.2 | 0.18 | 0.25 |
| $^{143}Nd/^{144}Ndm$ | 0.512333 ± 15 | | | | | 0.512305 ± 12 | | |
| $^{143}Nd/^{144}Ndi$ | 0.512325 | | | | | 0.512300 | | |
| $^{147}Sm/^{144}Nd$ | 0.104711 | | | | | 0.110685 | | |
| εNd (t) | −5.81 | | | | | −6.41 | | |
| TDM | 1.00 | | | | | 1.02 | | |
| $^{87}Sr/^{86}Srm$ | 0.70712 ± 3 | | | | | 0.70994 ± 3 | | |
| $^{87}Sr/^{86}Sri$ | 0.70701 | | | | | 0.70979 | | |

explained by mechanical fractionation of accessory minerals produced during transport/depositional processes.

Chondrite (Mc Donough and Sun, 1995)-normalized rare earth elements (Fig. 12a, b) yield patterns with a moderate slope, corresponding to $(La/Yb)_N$ between 17 and 10, exceptionally 8. $(La/Sm)_N$ ranges from 5.5 to 3.5 and the HREE define a slope of 2 to 1.3 $(Gd/Yb)_{N;}$ the patterns show no garnet as a residual phase. Eu/Eu* average is 0.69 for the ignimbrites indicating plagioclase fractionation, probably at shallow levels. Some slight differences in the MREE and HREE enrichment found within the Luingo ignimbrites could be related to variations in the amounts of mineral phases – such as hornblende and/or zircon – involved in the fractionation processes. The Lavas I show REE patterns very similar to those of the ignimbrites and the subtle differences could be related to different proportions of fractionation of mineral phases. For instance, a small variation in the amount of titanite can greatly modify these patterns. On the other hand, much more marked differences are evident when comparing with the samples from Lavas II, where the presence of garnet in the source is evident.

Chondrite (Mc Donough and Sun, 1995)-normalized multi-element diagrams (Fig. 12c, d) show a common behaviour for the ignimbrites of the Luingo caldera; a slight difference is marked by the higher concentration of Y and Yb in the Alto de Las Lagunas Ignimbrite. The lava flows of different age (Lavas I and Lavas II) are clearly separated also by their geochemical features; the middle Miocene Lavas I have patterns that resemble those of the ignimbrites, whereas the upper Miocene Lavas II show contrasting patterns. Lavas I have greater contents in Ba, Sr, P and Zr than the ignimbrites. These differences can be ascribed to different proportions of a subcrustal mafic end-member in the hybrid magma (Ba, Sr) and/or to different magma temperatures (higher P and Zr in Lavas I is consistent with higher T in these); or may also be related to different fractionation degrees of phases such as plagioclase and biotite. The Lavas II group has more prominent Nb–Ta anomalies (i.e., a more arc-like signature or more crustal component) and less content in Yb and Y (probably related to residual phases such as garnet and/or amphibole).

The PCTVC isotopic $^{87}Sr/^{86}Sr_i$ values are in the range of 0.70750 to 0.70918 and $^{143}Nd/^{144}Nd_i$ varies between 0.511230 and 0.512455. $^{87}Sr/^{86}Sr$ has positive correlation with $SiO_2$ and Rb/Sr thus indicating that not only fractional crystallization but also assimilation processes occurred. Nevertheless, the wide range of isotopic ratios and $T_{DM}$ values points to complex magmatic processes and is sufficient to discard closed-system magmatic evolution of the PCTVC.

From the geochemical analysis as a whole, some processes are evident: a) fractional crystallization, b) assimilation of crustal material (e.g., on the base of isotopic ratios), c) the presence of a mafic source during recharge that led to the high An % contents (more evident in the Arremo Unit). The latter is also consistent with other evidence, such as different compositional groups of the same mineral phases (e.g., biotite, spinels) within a given unit, and petrographic disequilibrium features.

Although the magmatic evolution of PCTVC must have included complex magmatic processes, probably with deep or intermediate magma chambers feeding the shallowest and ultimate magma chamber within the crust, as suggested for many other calderas in the Puna (e.g., de Silva et al., 2006), we performed a simplified model of the evolutive process in the last magma chamber only.

Together, the geochemical and petrographic features point to assimilation and fractional crystallization with recharge (AFC-r) as the most feasible process.

Before moving to AFC-r, we also made attempts (not shown) to model the Luingo samples by a mixing-only model, but, as expected, no successful results were found. For the AFC-r model we followed the formulation proposed by DePaolo (1981) and extended by Aitcheson and Forrest (1994). We first needed to decide which end members (i.e. initial magma composition and assimilant) and recharge magma to use. Because of the limited composition range of the PCTVC exposed rocks, adequate extreme compositions do not occur within the set of volcanic samples analyzed in this work. We therefore selected well known samples from both the local basement and basic rocks within the SCVZ.

For the original magma composition we chose to use the Las Maquinas Basalt (Kay et al., 1999), as it is a ca. 23 Ma back arc basalt

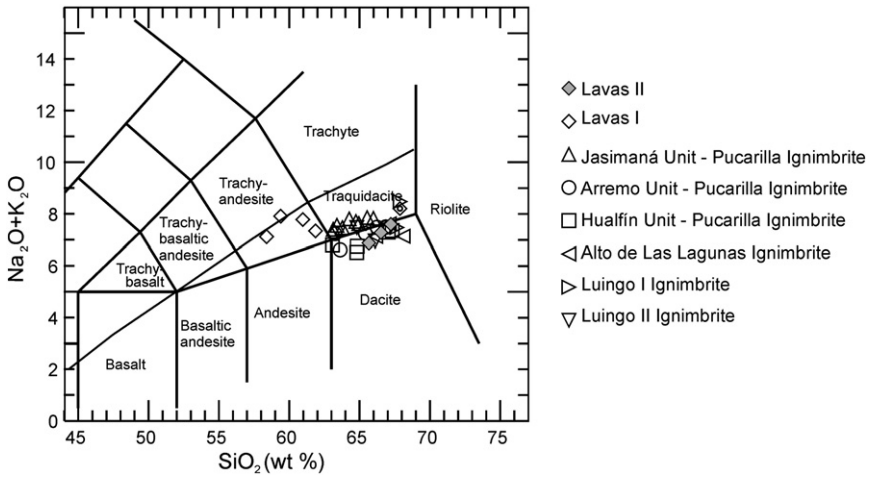


**Fig. 9.** Total Alcalis Silica (TAS) diagram (Le Maitre et al., 1989) showing the classification of rocks from the PCTVC.

that could represent the basic compositions previous to the major thickening event in this region. Among the results obtained by Caffe et al. (2002) using the Melts software (Ghiorso and Sack, 1995) we selected the theoretical paragenesis of this basalt at 5 kbar and F = 0.5 (fraction of magma remaining); i.e., CPx: 67%, Pl: 33% thus giving a $D_{Sr}$ of 1.46 and $D_{Nd} = 0.61$ (Table B1, Appendix B in Caffe et al. 2002). As the contaminant we use the average of selected Ordovician granitoids from Antofalla Salar (samples M18/1[a] and

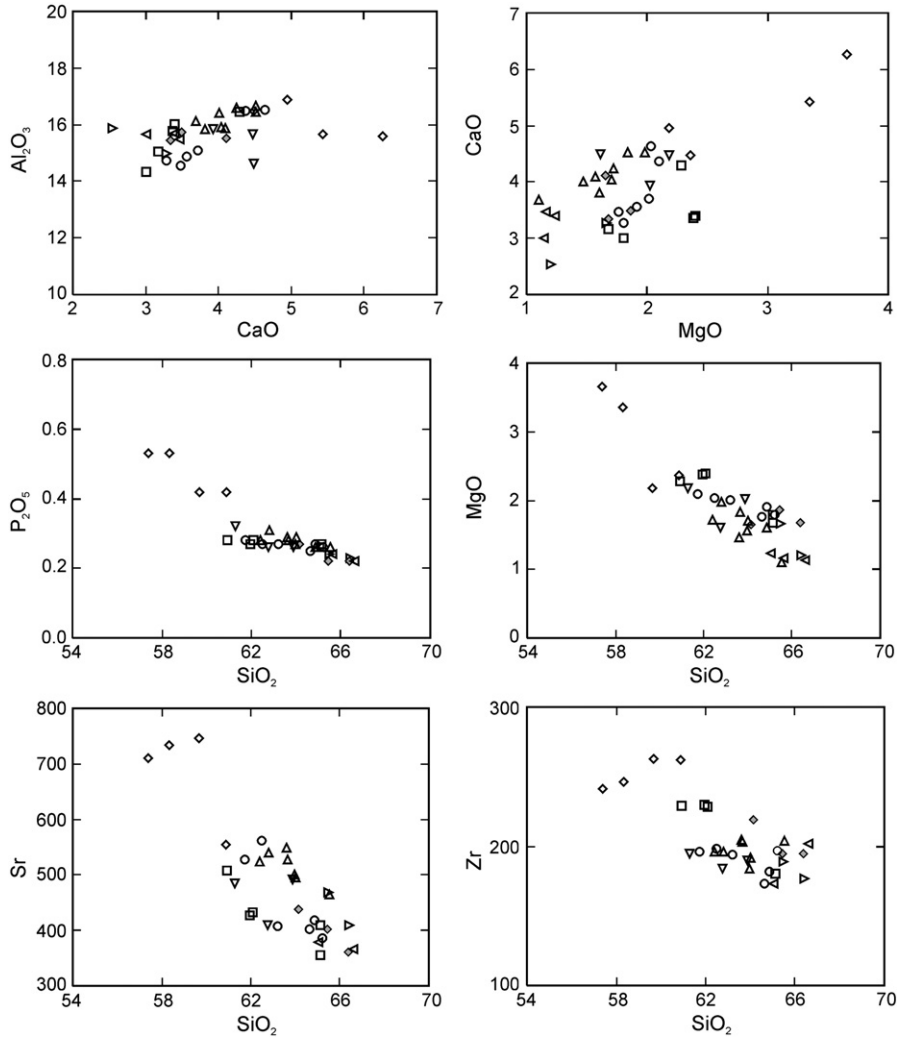


**Fig. 10.** Selected correlation diagrams of major and minor elements of rocks from the PCTVC. Symbols as in Fig. 10.

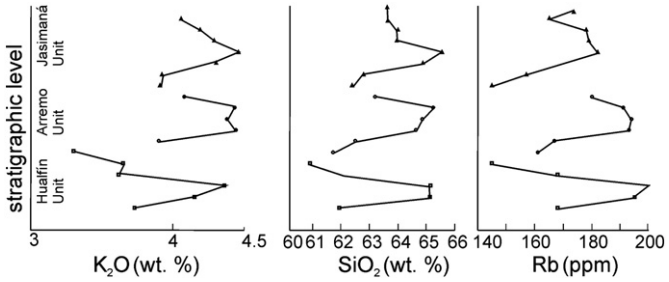


**Fig. 11.** Stratigraphic level variations of major and minor elements ($K_2O$, $SiO_2$, and Rb) within Pucarilla Ignimbrite.

M18/5[a] from Lucassen et al., 2001). Using the same simplification proposed by Aitcheson and Forrest (1994), we consider for the recharge magma the same composition as the original magma. The graphical method based on Equations (9) and (10) proposed by Aitcheson and Forrest (1994) leads to a family of triple solutions (β, r, ρ) where β = (rate of recharge)/(rate of assimilation), r = (rate of assimilation of crust)/(rate of fractional crystallization) and ρ = (crust)/(magma). However, as suggested by Aitcheson and Forrest (1994), using zero (i.e. no recharge, see Model 1 in Table 7) or low values for β in the presence of high values of bulk D (i.e. highly compatible elements), besides being in contrast with the geochemical evidence discussed above, can lead to an overestimation of ρ. Therefore, we consider that models with higher values of β are more plausible (see Models 2 and 3 in Table 7). Considering all the range of possible values of β, we always obtain percentages of crustal melts between 17 and 23%.

## 6. The Luingo caldera and its significance in the southern CVZ

The Luingo caldera is the easternmost large-volume magmatic complex of the CVZ. Its position and age allows constraining possible geochemical changes in the eastern Puna border with time and also evaluating the existence of geochemical variations from W to E during the middle Miocene.

### 6.1. Crustal thickening in time

During the last decades it has been proposed that the major thickening event within the Puna was about 10 m.y. ago (e.g., James, 1971; Isacks 1988). As the Luingo caldera (middle Miocene) is located close to the Cerro Galán Complex (ca. 6.5 to 2 Ma: e.g., Sparks et al., 1985; Folkes et al., submitted for publication) and is older than the generally accepted time of main thickening event in this area, we first compared our data with those of the younger Cerro Galán Complex (CGC). Some features that come to light from this comparison are a) variation diagrams show correlatable trends, CGC rocks being more evolved, b) REE diagrams show higher LREE and lower HREE for the CGC, i.e., the Luingo caldera magmas show no evidence for garnet as a residual phase, as opposed to what occurs in the Cerro Galán caldera (e.g., Kay et al., 2008), c) N-MORB-normalized multielement patterns of the Luingo caldera are similar to those of the CGC rocks, although the latter evidently contain lesser amounts of P, Ti and Sr, suggesting a

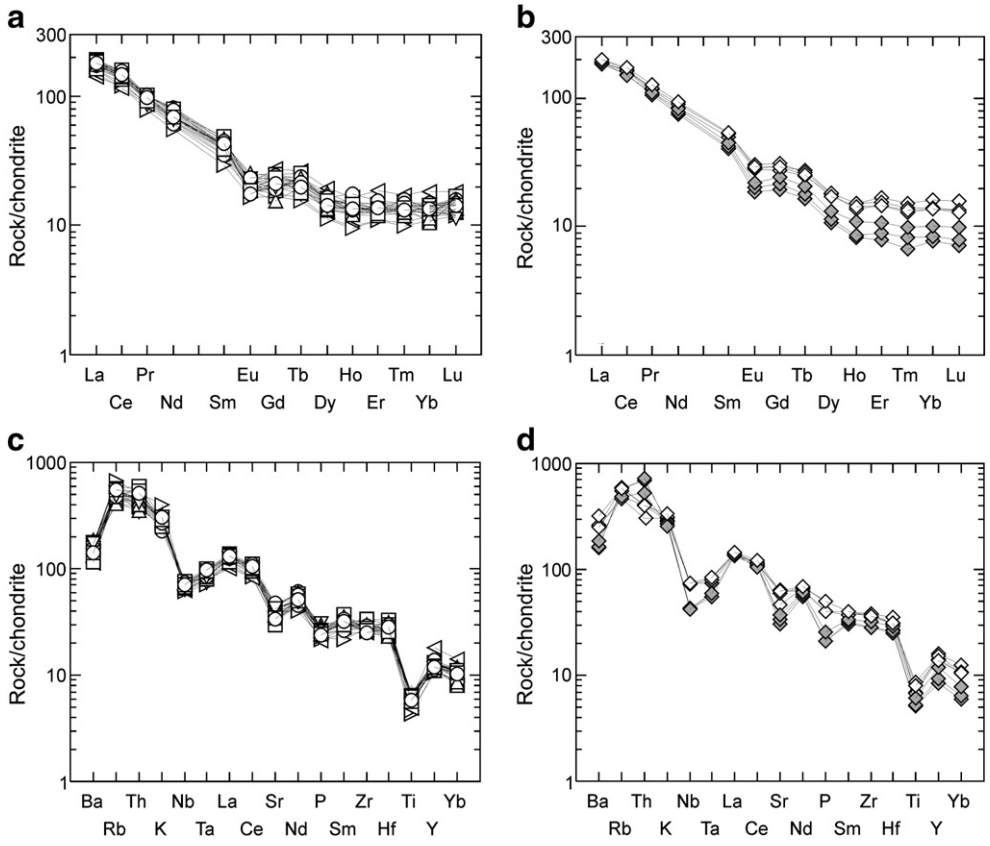


**Fig. 12.** Chondrite normalized REE (a, b) and multielement diagrams (c, d) diagrams showing (a, c) pyroclastic rocks from the Luingo caldera, (b, d) effusive units from the PCTVC. Normalization chondrite values for multielement diagrams from Thompson (1982), with alternative value for Ba (Hawkesworth et al., 1984); chondrite values for rare earth elements diagrams from (McDonough and Sun, 1995).

**Table 7**
AFC with recharge model. Original and recharge magma: Las Máquinas basalt. Contaminant: Average of selected Ordovician granitoids (Lucassen et al., 2001); see text. Bulk partition coefficient values as in Caffe et al. (2002) from clinopyroxene and plagioclase partition coefficients given in Bacon and Druitt (1988). The AFC-r models were calculated using DePaolo (1981) equations modified by Aitcheson and Forrest (1994). D (bulk partition coefficient); Ca (element concentration in wall-rock melt); C°m (element concentration in the original magma); εa (isotopic ratio in the wall-rock melt); ε°m (isotopic ratio in the original magma); εm (isotopic ratio in the contaminated magma). β, r and ρ defined in the text.

| Parameter | Sr | Nd | |
|---|---|---|---|
| D | 1.46 | 0.61 | |
| Ca | 71 (67–75) | 44 (41–47) | |
| C°m | 520 | 16 | |
| εa | 0.7561705 (0.751292–0.761049) | −13.295 (−13.38–13.21) | |
| ε°m | 0.70400 | 4 | |
| εm | 0.70834 (0.70750–0.70918) | −5.0985 (−6.63 a–3.567) | |
| Results | Model 1 | Model 2 | Model 3 |
| β | 0.00 | 0.75 | 1.45 |
| r | 0.37 | 0.30 | 0.17 |
| ρ | 0.30 | 0.28 | 0.20 |
| % assimilated crust | 23% | 22% | 17% |

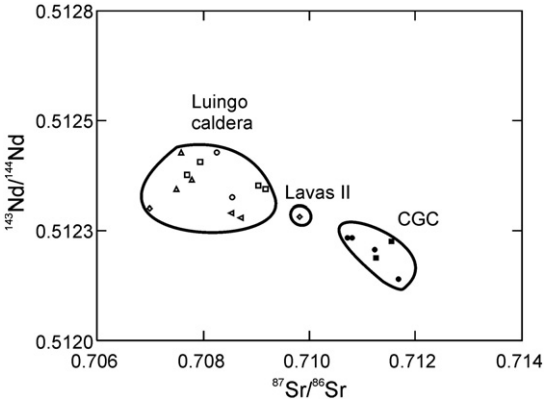


**Fig. 13.** $^{87}Sr/^{86}Sr$ vs $^{143}Nd/^{144}Nd$ plot of PCTVC and Cerro Galán Complex. PCTVC symbols as in precedent figures; CGC isotopic data (Francis et al., 1989): black squares represent Cerro Galán Ignimbrite and black circles represent upper Miocene ignimbrites of the Cerro Galán Complex.

greater degree of fractionation of certain mineral phases, d) Mg# are similar, indicating similar bulk crystal fractionation in both complexes.

On the other hand, Sr and Nd isotopic ratios (Fig. 13) show a progressive increase in $^{87}Sr/^{86}Sr$ and decrease in $^{143}Nd/^{144}Nd$ from the Luingo caldera rocks (middle Miocene), through Lavas II (upper Miocene), to CGC (upper Miocene to Pliocene), thus indicating an increase in the amount of assimilated component; different proportions and/or compositions of mantle — crustal melts with time (e.g. Kay et al. 2010). This is also confirmed by the AFC and AFC-r models, where the CGC is found to represent a mixture of 50:50 crustal/mantle melts (Kay et al., 2008) whereas Luingo caldera represents ca. 20:80 (this work).

We also selected representative samples from the Cerro Galán Ignimbrite (Pliocene: Folkes et al., submitted for publication), Blanco Ignimbrite (upper Miocene: Folkes et al., submitted for publication) and Luingo caldera ignimbrites (middle Miocene: this work) and plotted their chondrite-normalized REE (see Fig. 14a). Considering the presence of garnet in the source as indicative of crustal thickening (e.g., Coira et al., 1993), different REE trends and slopes are obvious from middle to upper Miocene, but less evident from upper Miocene to Pliocene. So, if we compare Blanco Ignimbrite (upper Miocene) with Galán Ignimbrite (Pliocene), their REE slopes are equal and the slight differences in their absolute content can be easily addressed by FC (e.g., Folkes et al., submitted for publication). This is reinforced if we compare Lavas II (upper Miocene) data (see Table 6) with the Cerro Galán Ignimbrite.

Overall, a higher proportion of crustal material is evident in the CGC (e.g., Kay et al., 2008), in comparison with the middle Miocene Luingo volcanic rocks. Furthermore, CGC magmas exhibit the presence of garnet as a residual phase in the source, which could be interpreted as the result of a thickened crust at this time (e.g., Coira et al., 2003; Kay et al., 2008). The same is true for the upper Miocene Lavas II from the PCTVC.

### 6.2. Geochemical assessment of arc configuration changes

If we consider a Miocene arc developed close to the present one, 230 km westward from both the Luingo and the Cerro Galán calderas, they are both set in a "back arc" position. This raises the opportunity to try and use geochemical tools to study changes in arc–back arc configuration, as started by Coira et al. (1993) and Kay et al. (1999). To highlight this, we compared the geochemical data from the Luingo caldera with those from other middle Miocene volcanic rocks of the Southern CVZ (25–27 S), set between 67 and 69°W. The aim of this comparison is to assess whether geochemical evidence is enough to accurately constrain the arc–back arc position and/or arc width/configuration for middle Miocene times.

It is known that continental arc magmas generally show an enrichment in LIL elements in relation with the concentrations of HFSE (e.g., McDowell and Clabaugh, 1979; Pearce, 1983); this behaviour is basically related to the affinities of these elements with the fluid phases. Through a comparison with the available (Baker et al., 1987; Mpodozis et al., 1995; Kraemer et al., 1999; Trumbull et al., 1999; Siebel et al., 2001; Schnurr et al., 2007) geochemical data over the 25–27° segment of the CVZ it comes out that N-MORB-normalized patterns vary from west to east (this is just a tendency and we need to emphasize that all these element concentrations overlap in the samples from the west and east), showing differences in Th, Ba, Nb and Ta that may mostly reflect the participation of fluid phases in the astenospheric wedge. However, mineral phases as rutile, titanite, feldspars and ilmenite can also affect the concentrations of these elements. Differences in Zr, P, Sr, Ti and Y are also found and can reflect variable fractionation degrees of mineral phases (e.g. amphibole, ilmenite) and/or different proportions of mafic end-members.

Our results show that as was previously pointed by other authors (e.g., Saunders and Tarney, 1984; Davidson and de Silva, 1995; Siebel et al., 2001; Caffe et al., 2002; Schnurr et al., 2007) there is a tendency in the CVZ for Nb concentration to increase, and for Zr/Nb and Ba/Nb to decrease eastward. These variations have been interpreted as a result of variable basement composition from west to east (Schnurr et al., 2007) and/or a decrease in subduction-related signature (Siebel et al., 2001; Caffe et al., 2002); and as variable sources and depth in the Benioff zone (Davidson and de Silva, 1995). It is reasonable to argue that these differences can only reflect different settings if rocks of similar ages are considered (see. e.g., Fig. 13). For instance, it is true that Nb (and Ta) increase eastwards if we compare rocks of the 67–69°W SCVZ with the ones of the Luingo caldera but this is not the case for the Cerro Galán Complex (where they overlap). If this eastward Nb increase and Ba/Nb decrease reflect a progressively increasing distance of the magmas from the arc, it is not possible to explain the differences between Cerro Galán caldera and Luingo caldera which are spatially close, unless a significative time span is considered. This same time-dependence is found if strontium isotopic ratios (e.g., Schnurr et al., 2007) are used as a tool for discrimination between arc and back arc settings. It can also be argued that these ratios and concentrations depend greatly on the petrologic evolution of each volcanic centre, the source of their parental magmas (e.g., Kay et al. 2010, invoke the presence of mineral phases that retain Nb in the source of Galan's ignimbrites) and/or the degree in which crustal

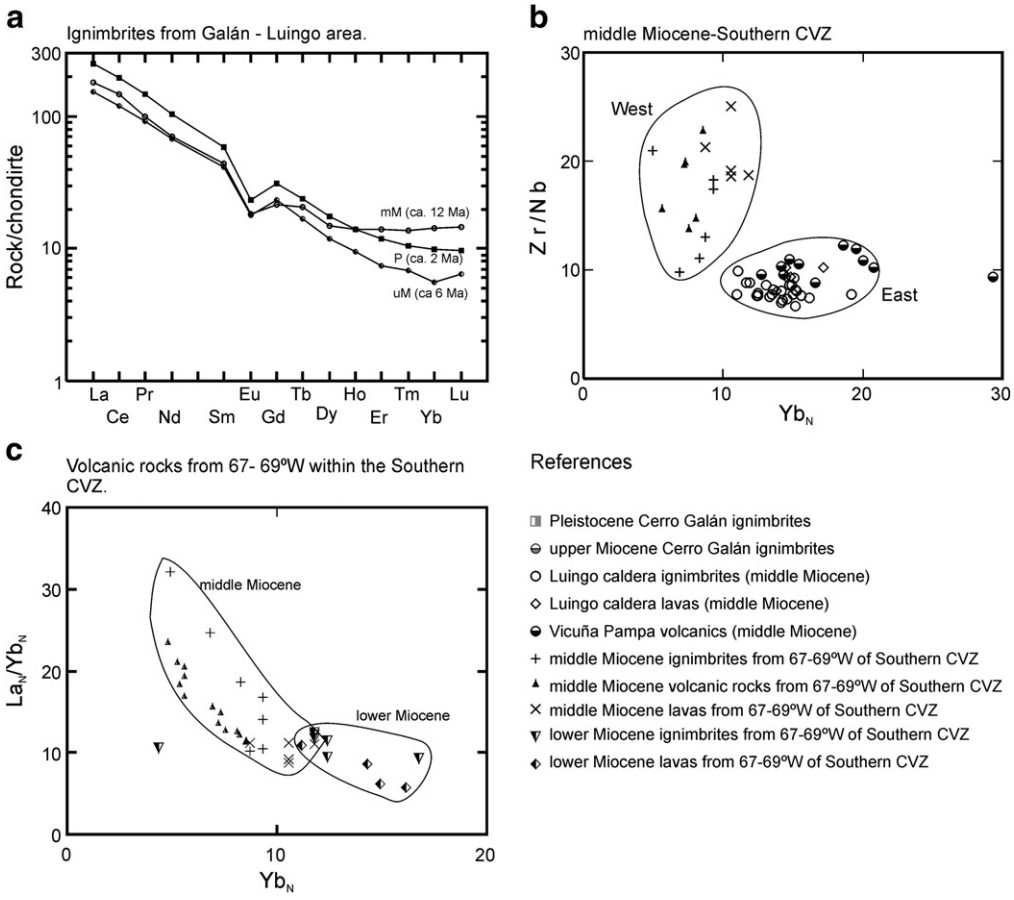


**Fig. 14.** (a) REE diagram showing volcanic rocks from CGC and PCTVC; (b) Zr/Nb vs. $Yb_N$ diagram displaying middle Miocene volcanic rocks from the Southern CVZ (25–27°S); (c) $La_N/Yb_N$ vs. $Yb_N$ showing middle and upper Miocene volcanic rocks of the west portion of the Southern CVZ (67–69°). Geochemical data from Baker et al., 1987; Mpodozis et al., 1995; Kraemer et al., 1999; Trumbull et al., 1999; Siebel et al., 2001; Schnurr et al., 2007; Folkes et al., submitted for publication; this work.

melts were involved (e.g., Davidson and de Silva, 1995 and references therein).

In order to assess geochemical differences between middle Miocene volcanic centres from west to east, we compare the felsic ignimbrites and andesitic lavas of Southern CVZ (Baker et al., 1987; Mpodozis et al., 1995; Kraemer et al., 1999; Trumbull et al., 1999; Siebel et al., 2001; Schnurr et al., 2007) with the Luingo caldera and the mafic volcanic rocks of Vicuña Pampa (unpublished data) to the east. Differences are best visible when plotting $Yb_N$ vs. Zr/Nb (Fig. 14b), thus indicating that these variables are efficient tools to constrain E–W geochemical differences for the middle Miocene in the Southern CVZ. Furthermore, the western samples have more pronounced HREE slopes (generally $Gd_N/Yb_N = 2.64–4.6$; exceptionally $Gd_N/Yb_N = 1.76$) than the eastern ones ($Gd_N/Yb_N = 1.31–1.78$). $Yb_N$ variations can be attributed to different crustal thickness and/or to different depths of magma sources within the mantle, i.e., garnet–lherzolite stability field for the western samples and spinel–lherzolite stability field for the eastern ones. Moreover, the differences in the Zr/Nb ratio may reflect differences in subduction-related signature as suggested by Siebel et al. (2001) and Caffe et al. (2002).

As we found differences in volcanic rocks at the same longitude for different ages and at different longitudes for the same age, we must now search for possible differences between rocks of different ages in the western portion of the Southern CVZ. The results show that the same HREE depletion that we found in the upper Miocene–Pliocene with respect to the middle Miocene in the eastern zone, are found between middle Miocene (11–16 Ma) with respect to lower Miocene (>16 Ma) in the west (samples from Siebel et al., 2001 and Schnurr et al., 2007, see $Yb_N$ vs. $La/Yb_N$ plot in Fig. 14c), with the exception of one isolated sample.

## 7. Discussion and concluding remarks

The middle Miocene Luingo volcanic rocks can be modelled by a mixture of ca. 80% mafic magmas and 20% of crustal melts by AFC-r process. On the other hand rocks from the nearby Cerro Galán caldera were modelled by mixtures of 50:50 mantle/crust melts (Kay et al., 2008). These differences in the crustal/mafic ratios of Cerro Galán ignimbrites with respect to the one of Luingo caldera, are better explained by the higher crustal component in those rocks (e.g., Kay et al., 2008), which have more evolved magmas and more radiogenic Sr isotopes. Moreover, a significant difference between Luingo and Cerro Galán rocks is the mantelic signature of the mafic component as shown in REE patterns. In the case of Cerro Galán caldera REE patterns indicate the presence of garnet as a residual phase in the source (e.g., Kay et al., 2008), whereas the mafic magmas that were involved in the Luingo caldera's magma evolution do not suggest the presence of garnet in the source of those magmas (see Fig. 14a). Steep REE patterns in the Puna–Altiplano volcanic rocks were interpreted as a result of the presence of garnet in the source but a more striking interpretation is that this points to a thickened crust (e.g., Coira and Kay, 1993). If this is true, then this thickened crust should have been present at least since the Lavas II event (upper Miocene), but not at the Luingo caldera event (13–12 Ma).

Although it is highly accepted that the processes leading to the crustal thickening and uplift of the Altiplano–Puna Plateau have been active since at least the Eocene–Oligocene along both western and eastern margins (e.g., Mpodozis et al., 2005; Carrapa et al., 2005; Arriagada et al., 2006; Hongn et al. 2007); palaeoclimatic and palaeoaltimetric data in the northern Altiplano (Gregory-Wodzicki, 2002; Garzione et al., 2006; Molnar and Garzione, 2007; Hoke and

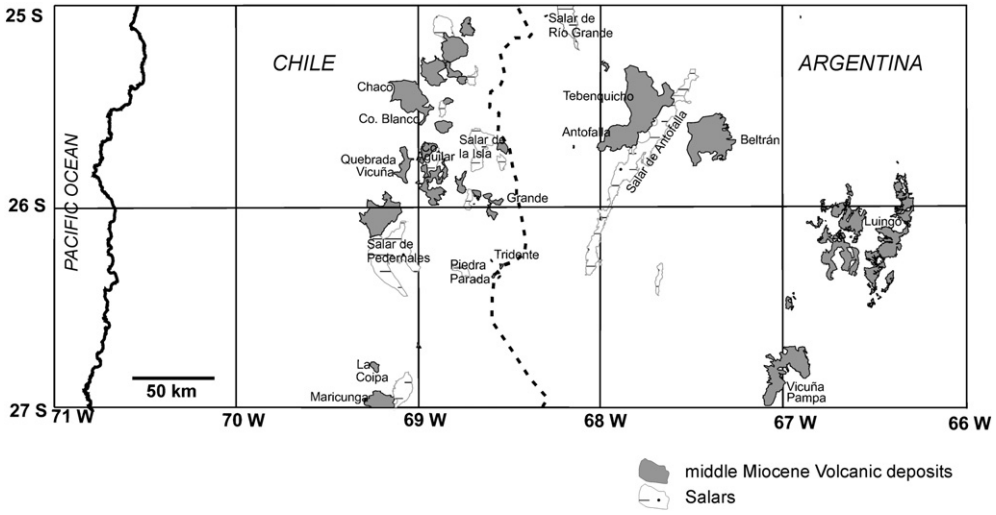


**Fig. 15.** Map showing areal distribution of middle Miocene (11–16 Ma) volcanic products within the Southern CVZ.

Garzione, 2008) point to a rapid uplift during the upper Miocene, as it was earlier suggested by James (1971) and Isacks (1988).

The comparison of geochemical data of middle Miocene volcanic rocks from west to east suggests that at this time the crust was thicker in the western than in the eastern portion of the Southern CVZ. It is tempting to interpret that the process of crustal thickening was accelerated in the western portion during the middle Miocene and then in the eastern portion of this part of the Puna during the upper Miocene (ca. 10 Ma).

Besides the geochemical evidence, it is important to recognize the areal distribution of volcanic rocks in the Southern CVZ to compare the variations in the magnitude of volcanism from west to east. With the available data from the literature we constructed a map (Fig. 15) with the volcanic rocks of 11–16 Ma. From this figure it is evident that the volcanic deposits, but not necessarily the volcanic centres, have a NNE–SSW trending, which can be related with dominant ranges that were aligned in that direction during the middle Miocene and/or by post middle Miocene NNE–SSW trending faults (e.g., Mon and Salfity, 1995; Adelmann and Görler, 1998; Riller and Oncken, 2003) that would have produced this same configuration. Interestingly, volcanic occurrences appear to be restricted to the west and east Puna margins, and in a middle position following the trend of the structurally-controlled Antofalla basin (Adelmann and Görler, 1998). Thus, we argue that it is not appropriate to refer to a main arc for the deposits in the western sector. Instead it is more prompting to envisage a broad arc, structurally controlled in both proto-Puna/Puna margins, in which the geochemical differences are related with variations in the crustal thicknesses and heterogeneous mantle magmatic sources from west to east, perhaps also related with these crustal thickness variations.

## Acknowledgements

This research was funded by PIP 5255 and PIP 781 (CONICET), PICT 2006-381 (ANPCyT), CIUNSa 1810, CNPq (306650/2007-0) and CAPES-SECyT BR/PA05-UVII014, projects. Datings funded by DFG Leibniz Institute for Surface Process and Climate Studies (STR373/16-1) for which special thanks are given to M. Strecker. C. del Papa helped with comments and fieldwork. Thanks to A. Nieva, R. Dominguez, R. Pereyra, O. Rodrigues Nunes, J. Chaves, B. Lima, and S. Ferraz Araujo for technical assistance. S. Guzmán thanks N. Hauser and G. da Silva Bispo Pereira for performing some analyses. We finally acknowledge the precious comments by P. Caffe and G. Aguirre-Díaz, which considerably improved the original manuscript.

## Appendix A. Analytical techniques

Age determinations by $^{40}Ar/^{39}Ar$ method were carried out in two fresh biotite samples from Lavas II Unit at the geochronology laboratory in the University of Potsdam. Biotite separates were obtained at the Universidad Nacional de Salta laboratory in Argentina following standard techniques (i.e., crushing, milling, sieving, and mineral separation by a Frantz Magnetic Separator, followed by separation with paper shaking, cleaning in an ultrasonic bath, drying at 80°–100 °C over 24 h, and handpicking under a binocular microscope). Neutron activation of the samples was performed at the GKSS FRG-1 research reactor, Geesthacht Neutron Facility (GeNF), Germany, where the samples were irradiated over 96 h (4 days) with a fast neutron flux of $1\times10^{12}$ n/cm$^2$/s, with the aim of obtaining enough $^{39}Ar$ from the $^{39}K$ (n, p) $^{39}Ar$ nuclear reaction. As an age standard sample, sanidine from the Fish Canyon Tuff was irradiated together with our samples in order to obtain J values, that reflect the degree of neutron activation. The sanidine had been dated at the Geological Survey of Japan, providing an age of 27.5 Ma (Uto et al., 1997; Ishizuka et al., 2002). After one month, the samples had been cooled down at the GeNF and were ready for Ar isotopic analysis at the University of Potsdam. The laboratory's Ar analytical system integrates a New Wave Gantry Dual Wave laser ablation system with a 50 W $CO_2$ laser (wavelength: 10.6 μm) for heating samples and extracting gas. In addition, the system contains an ultra-high vacuum purification line with Zr–Al alloy SAES getters and a cold trap maintained at the freezing temperature of ethanol, as well as a Micromass 5400 sector-type noble gas mass spectrometer, which has a high sensitivity and an ultra-low background. Samples were analyzed by stepwise heating. The biotite grains were heated by a $CO_2$ laser beam for periods of between 1 and 1.5 min per step. The Ar isotopic analysis during stepwise heating was repeated until total fusion of the sample had occurred. The age was then calculated following the methodology of Uto et al. (1997). For each irradiation two biotite K–Ar age standards, SORI93 biotite (92.6 ± 0.6 Ma; Sudo et al., 1998) and HD-B1 biotite (24.21 ± 0.32 Ma; Hess and Lippolt, 1994) were irradiated and the $^{40}Ar/^{39}Ar$ ages measured, in order to confirm the accuracy of the dating system in each irradiation. Results were entered in an Excel spreadsheet, where several corrections were performed including system blank, mass discrimination, post-irradiation decay of $^{37}Ar$ and $^{39}Ar$, and neutron-induced interferences from Ca and K. We thus obtained plateau, isochron, and total-gas ages. Steps for plateau determination were performed following McDougall and Harrison (1999) recommendations. Used criterion to determine

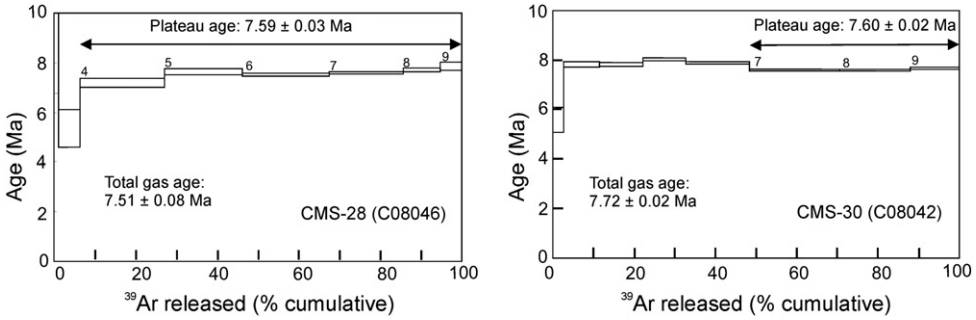


**Fig. 16.** Biotite $^{40}Ar/^{39}Ar$ age spectra obtained by stepwise heating experiments. Numbers refer to steps used for the calculation of the plateau ages. Uncertainties are given in 1 sigma without J value error.

the plateau steps are involved in McDougall and Harrison (1999) These are, (1) the ages of two consecutive steps should agree to within ± 2 sigma, excluding the J value error, (2) the total plateau length should include more than 50% of the total $^{39}Ar$ released, and (3) each degassing step making up the plateau should comprise at least 3% of the total $^{39}Ar$ released. $^{40}Ar/^{39}Ar$ results are shown in Fig. 16 and listed (± 1 sigma) in Table 8.

Chemical analyses of selected minerals were performed by WDS with a Cameca SX-50 electron microprobe equipped with 4 WDS spectrometers, operating at 25 nA and 16 KeV, in most cases with a beam size of 1 μm, at the Instituto de Geociências, Universidade de Brasilia. Equipment was calibrated with a combination of natural and synthetic standards. The analytical errors are below 2% of the concentration for major elements and below 5% of the concentration for minor elements.

Selected samples were processed at the Universidad Nacional de Salta Geochemical laboratory, where they were crushed and milled. All analyses were performed on fresh samples; pumice fragments from ignimbrites were separated when possible. Major and some minor elements were determined by X-ray fluorescence (FRX) at the LANAIS laboratory (Universidad Nacional de Salta, Argentina) on a RIGAKU 2000 with a dispersive wavelength and Rb tube, PC gas flux, SC detector and monochromatic crystals: LIF PET, TAP and GE. Ground and homogenized samples were fused with lithium tetraborate as a flux for major element analyses. Trace elements were determined in rock powder pellets mixed with methacrylate and pressed at 1400 kg/cm$^2$. Major and trace elements were analyzed by standard methods, using standards from Geological Survey of Japan and United States Geological Survey. Loss on ignition was determined by weight difference after heating at 1000 °C. Rare earth elements (REE) and other trace elements (ppm) were quantitatively and qualitatively determined at the ACME (Canada) laboratory by ICP-MS (Inductively Coupled Plasma-Mass Spectrometer) and others by ICP-AES (Inductively Coupled Plasma-Atomic Emission Spectrometer), samples were

**Table 8**
$^{40}Ar/^{39}Ar$ results on biotite samples Lavas II.

CMS-28 (C08046)

| J = 0.001999 | | $^{40}Ar/^{39}Ar$ | $^{37}Ar/^{39}Ar$ | $^{36}Ar/^{39}Ar$ ($\times10^{-3}$) | K/Ca | $^{40}Ar^*$ (%) | $^{39}Ar_K$ fraction (%) | $^{40}Ar^*/^{39}Ar_K$ | Age(± s) (Ma) |
|---|---|---|---|---|---|---|---|---|---|
| Steps | Laser output | | | | | | | | |
| 1 | 1.6% | 11,606.313 ± 985.514 | 2.888 ± 1.572 | 38,480.538 ± 3269.494 | 0.20 | 2.03 | 0.01 | 236.284 ± 43.124 | 697.90 ± 105.65 |
| 2 | 2.2% | 322.348 ± 1.698 | 0.006 ± 0.009 | 1080.952 ± 6.522 | 95.35 | 0.91 | 1.11 | 2.928 ± 1.046 | 10.53 ± 3.75 |
| 3 | 2.8% | 68.034 ± 0.068 | 0.005 ± 0.001 | 225.214 ± 0.730 | 118.57 | 2.18 | 5.28 | 1.484 ± 0.209 | 5.34 ± 0.75 |
| 4 | 3.2% | 17.933 ± 0.031 | 0.003 ± 0.003 | 53.934 ± 0.185 | 230.46 | 11.13 | 20.67 | 1.996 ± 0.053 | 7.19 ± 0.19 |
| 5 | 3.6% | 11.382 ± 0.013 | 0.029 ± 0.004 | 31.360 ± 0.115 | 20.11 | 18.62 | 19.12 | 2.119 ± 0.034 | 7.63 ± 0.12 |
| 6 | 4.0% | 5.766 ± 0.007 | 0.038 ± 0.003 | 12.469 ± 0.045 | 15.57 | 36.18 | 21.19 | 2.086 ± 0.013 | 7.51 ± 0.06 |
| 7 | 4.4% | 4.368 ± 0.005 | 0.017 ± 0.002 | 7.648 ± 0.032 | 35.41 | 48.31 | 18.17 | 2.110 ± 0.010 | 7.59 ± 0.05 |
| 8 | 4.8% | 4.663 ± 0.006 | 0.013 ± 0.003 | 8.536 ± 0.065 | 46.12 | 45.94 | 9.18 | 2.142 ± 0.019 | 7.71 ± 0.08 |
| 9 | 5.2% | 4.364 ± 0.012 | 0.031 ± 0.007 | 7.394 ± 0.153 | 19.25 | 50.02 | 5.27 | 2.183 ± 0.046 | 7.86 ± 0.17 |

CMS-30 (C08042)

| J = 0.001999 | | $^{40}Ar/^{39}Ar$ | $^{37}Ar/^{39}Ar$ | $^{36}Ar/^{39}Ar$ ($x10^{-3}$) | K/Ca | $^{40}Ar^*$ (%) | $^{39}Ar_K$ Fraction (%) | $^{40}Ar^*/^{39}Ar_K$ | Age(± 1 s) (Ma) |
|---|---|---|---|---|---|---|---|---|---|
| Steps | Laser output | | | | | | | | |
| 1 | 1.6% | 709.817 ± 4.657 | 0.101 ± 0.080 | 2361.936 ± 15.700 | 5.80 | 1.67 | 0.14 | 11.878 ± 0.823 | 42.34 ± 2.90 |
| 2 | 2.2% | 96.792 ± 0.169 | 0.135 ± 0.010 | 322.377 ± 0.570 | 4.37 | 1.60 | 2.58 | 1.547 ± 0.139 | 5.57 ± 0.50 |
| 3 | 2.8% | 14.171 ± 0.022 | 0.055 ± 0.003 | 40.628 ± 0.097 | 10.71 | 15.33 | 8.71 | 2.172 ± 0.029 | 7.82 ± 0.11 |
| 4 | 3.2% | 7.173 ± 0.013 | 0.037 ± 0.003 | 16.945 ± 0.059 | 15.70 | 30.26 | 10.70 | 2.171 ± 0.018 | 7.81 ± 0.07 |
| 5 | 3.6% | 6.356 ± 0.007 | 0.053 ± 0.004 | 13.994 ± 0.061 | 11.10 | 35.04 | 10.53 | 2.227 ± 0.018 | 8.01 ± 0.07 |
| 6 | 4.0% | 6.120 ± 0.004 | 0.070 ± 0.003 | 13.342 ± 0.030 | 8.43 | 35.72 | 15.74 | 2.186 ± 0.009 | 7.87 ± 0.05 |
| 7 | 4.4% | 4.923 ± 0.007 | 0.043 ± 0.001 | 9.555 ± 0.013 | 13.52 | 42.76 | 22.16 | 2.105 ± 0.006 | 7.58 ± 0.04 |
| 8 | 4.8% | 4.010 ± 0.003 | 0.035 ± 0.002 | 6.456 ± 0.023 | 16.93 | 52.53 | 17.33 | 2.106 ± 0.007 | 7.58 ± 0.04 |
| 9 | 5.2% | 3.610 ± 0.006 | 0.020 ± 0.003 | 5.035 ± 0.027 | 29.24 | 58.85 | 12.11 | 2.124 ± 0.009 | 7.65 ± 0.04 |

| Sample | Unit | Location | | Material dated | Plateau age | | | | Isochron age | | | | | | Integrated age | | |
|---|---|---|---|---|---|---|---|---|---|---|---|---|---|---|---|---|---|
| | | Latitute | Longitude | | Age (Ma) | 1σ | $^{39}Ar$ (%) | *steps | Age (Ma) | 1σ | $^{40}Ar/^{36}Ar$ intercept | 1σ | *steps | MSWD | Age (Ma) | 1σ | Ca/K |
| CMS-28 | Lavas II | 27 06 47S | 66 40 25.7 W | Biotite | 7.59 | 0.03 | 93.6 | 6 (9) | 7.66 | 0.06 | 293.72 | 0.92 | 6 (9) | 1.52 | 7.51 | 0.08 | 0.00 |
| CMS-30 | Lavas II | 26 09 19S | 66 42 51.5 W | Biotite | 7.60 | 0.02 | 51.6 | 3 (9) | 7.67 | 0.07 | 292.63 | 2.12 | 3 (9) | 1.27 | 7.72 | 0.02 | 0.10 |

fused with lithium metaborate/tetraborate and solved and diluted in nitric acid. Detection limits are 0.1 to 0.01 ppm for REE and of 0.1 to 1 ppm for other trace elements.

The bulk-rock Sm–Nd isotopic analyses were carried out at the Geochronology Laboratory of the University of Brasília. Sample dissolution was carried in Teflon Savillex beakers or in Parrtype Teflon bombs. Sm and Nd extraction from whole-rock powders concentrates followed the technique of Gioia and Pimentel (2000), in which the separation of the REE as a group using cation-exchange columns precedes reversed-phase chromatography for the separation of Sm and Nd using columns loaded with HDEHP (di-2-ethylhexyl phosphoric acid) supported on Teflon powder. REE and Sm–Nd separation was performed using RE-Spec and Ln-Spec resins. A mixed $^{149}Sm$–$^{150}Nd$ spike was used. Sm and Nd samples were loaded onto Re filaments of a double filament assembly. Sm and Nd isotopic analyses were carried out using a Finnigan MAT-262 mass spectrometer. Uncertainties on Sm/Nd and $^{143}Nd/^{144}Nd$ ratios are considered to be better than $\pm 0.05\%$ ($1\sigma$) and $\pm 0.003\%$ ($1\sigma$), respectively, based on repeated analyses of international rock standards BCR-1 and BHVO-1. The $^{143}Nd/^{144}Nd$ ratios were normalized to a $^{146}Nd/^{144}Nd$ ratio of 0.7219. The Nd procedure blanks were smaller than 100 pg.

## References


Aceñolaza, F.G., Toselli, A.J., González, O., 1976. Geología de la región comprendida entre el salar del Hombre Muerto y Antofagasta de la Sierra, Provincia de Catamarca. Rev. Asoc. Geol. Argent. 31 (2), 127–136.

Adelmann, D., Görler, K., 1998. Segmentation of the Andean foreland in the Southern Puna, Central andes: sedimentary record from the Salar de Antofalla area, NW Argentina. Terra Nostra 98 (5), 4.

Aitcheson, S.J., Forrest, A.H., 1994. Quantification of crustal contamination in open magmatic systems. J. Petrol. 35, 461–488.

Allmendinger, R., 1986. Tectonic development, southeastern border of the Puna plateau, northwestern Argentina Andes. Geol. Soc. Am. Bull. 97, 1070–1082.

Allmendinger, R., Gubbels, T., 1996. Pure and simple shear plateau uplift, Altiplano–Puna, Argentina and Bolivia. Tectonophys. 259, 1–13.

Allmendinger, R.W., Jordan, T.E., Kay, S.M., Isacks, B.L., 1997. The evolution of the Altiplano–Puna Plateau of The Central Andes. Ann. Rev. Earth Planet. Sci. 25, 139–174.

Arriagada, C., Cobbold, P.R., Roperch, P., 2006. Salar de Atacama basin: a record of compressional tectonics in the Central Andes since the mid-Cretaceous. Tectonics 25. doi:10.1029/2004TC001770.

Bacon, C.R., Druitt, T.H., 1988. Compositional evolution of the zoned calcalkaline magma chamber of Mount Mazama Crate Lake, Oregon. Contrib. Mineral. Petrol. 98, 224–256.

Baker, M.C.W., Francis, P.W., 1978. Upper Cenozoic volcanism in the Central Andes — ages and volumes. Earth Planet. Sci. Lett. 41, 175–187.

Baker, P., Gonzales Ferrán, O., Rex, D., 1987. Geology and geochemistry of the Ojos del Salado volcanic region, Chile. J. Geol. Soc. 144, 85–96.

Blasco, G., Zappettini, E., 1996. Hoja Geológica 2566-I (1:250,000) San Antonio de los Cobres, provincias de Salta y Jujuy. Dirección Nacional del Servicio Geológico, boletín No 217, Buenos Aires, p. 126.

Caffe, P.J., Trumbull, R.B., Coira, B.L., Romer, R.L., 2002. Petrogenesis of early volcanic phases in Northern Puna Cenozoic magmatism. Implications for magma genesis and crustal processes in the Central Andean Plateau. J. Petrol. 43, 907–942.

Carrapa, B., Adelmann, D., Hilley, G., Mortimer, E., Sobel, E., Strecker, M., 2005. Oligocene range uplift and development of plateau morphology in the southern central Andes. Tectonics 24, TC4011. doi:10.1029/2004TC001762.

Carrera, N., Muñoz, J.A., 2008. Thrusting evolution in the southern Cordillera Oriental (northern Argentine Andes): constraints from growth strata. Tectonophys. 459 (1–4), 107–122.

Castillo, A. L., 1999. El Complejo Granítico Peñas Blancas, Jasimaná, Salta: petrografía y mineralizaciones. 14° Congreso Geológico Argentino, Actas 2, La Plata, pp. 155–158.

Coira, B., Kay, S.M., 1993. Magmatismo y levantamiento de la Puna, su relación con cambios en el ángulo de subducción y en el espesor cortical. 12° Congreso Geológico Argentino y 2° Congreso de Exploración de Hidrocarburos Actas 3, pp. 308–319.

Coira, B., Kay, S., Viramonte, J., 1993. Upper Cenozoic magmatic evolution of the Argentine Puna — a model for changing subduction geometry. Int. Geol. Rev. 8, 677–720.

Davidson, J.P., de Silva, S.L., 1995. Late Cenozoic magmatism of the Bolivian Altiplano. Contrib. Mineral. Petrol. 119, 387–408.

DePaolo, D., 1981. Trace element and isotopic effects of combined wallrock asimilation and fractional crystallization. Earth Planet. Sci. Lett. 53, 189–202.

de Silva, S.L., 1989. Altiplano–Puna Volcanic Complex of the Central Andes. Geology 17, 1102–1106.

de Silva, S.L., Francis, P.W., 1991. Volcanoes of the Central Andes. Springer-Verlag, Berlin.

de Silva, S., Zandt, G., Trumbull, R., Viramonte, J.G., Salas, G., Jiménez, N., 2006. Large ignimbrite eruptions and volcano-tectonic depressions in the Central Andes: a thermomechanical perspective. In: Troise, C., De Natale, G., Kilburn, C.R. (Eds.), Mechanism of activity and unrest at large calderas. Geological Society Special Publications, London, pp. 47–63. 269.

Devine, J.D., Rutherford, M.J., Norton, G.E., Young, S.R., 2003. Magma storage region processes Inferred from geochemistry of Fe–Ti oxides in Andesitic Magma, Soufriere Hills Volcano. Montserrat. J. Petrol. 44 (8), 1375–1400.

Droop, G.T.R., 1987. A general equation for estimating $Fe^{3+}$ in ferromagnesian silicates and oxides from microprobe analysis, using stoichiometric criteria. Mineral. Mag. 51, 431–437.

Folkes, C., Wright, H.M., Cas, R.A.F., de Silva, S.L., Lesti, C., Viramonte, J.G., submitted for publication. A re-appraisal of the stratigraphy and deposit volumes in the Cerro Galán volcanic system, NW Argentina. Bull. Volcanol.

Francis, P.W., Sparks, R.J., Hawkesworth, C.J., Thorpe, R.S., Pyle, D.M., Tait, S.R., Mantovani, M.S., McDermoth, F., 1989. Petrology and geochemistry of volcanic rocks of the Cerro Galán caldera, NW Argentina. Geol. Mag. 126 (5), 515–547.

Garzione, C.N., Molnar, P., Libarkin, J., MacFadden, B., 2006. Rapid late Miocene rise of the Bolivian Altiplano: evidence for removal of mantle lithosphere. Earth Planet. Sci. Lett. 241, 543–556.

Ghiorso, M.S., Sack, R.O., 1995. Chemical mass-transfer in magmatic processes 4. A revised and internally consistent thermodynamic model for the interpolation and extrapolation of liquid–solid equilibria in magmatic systems at elevated temperatures and pressures. Contrib. Mineral. Petrol. 119, 197–212.

Gioia, S.M.C.L., Pimentel, M.M., 2000. The Sm–Nd isotopic method in the Geochronology Laboratory of the University of Brasília. An. Acad. Bras. Ciênc. 72, 219–245.

González, O. E., Viruel, M. E., Fernández, D. S., 1999. El complejo piroclástico Cerro Tipillas en el borde oriental de la Puna Austral, Argentina. 14° Congreso Geológico Argentino, Actas 2, La Plata, pp. 236–239

Gregory-Wodzicki, K.M., 2002. A late Miocene subtropical-dry flora from the northern Altiplano. Bolivia. Palaeogeogr. Palaeoclimatol. Palaeoecol. 180 (4), 331–348.

Gubbels, T., Isacks, B., Farrar, E., 1993. High-level surfaces, plateau uplift, and foreland development, Bolivian Central Andes. Geology 21, 695–698.

Guzmán, S., 2009. Petrología y relaciones tectono-magmáticas del Complejo Volcánico Pucarilla – Cerro Tipillas. Thesis, Universidad Nacional de Salta, Argentina, Provincia de Salta. Ph. D.

Guzmán, S., Petrinovic, I., 2008. Pucarilla–Cerro Tipillas Volcanic Complex: the oldest recognized caldera in the southeastern portion of Central Volcanic Zone of Central Andes? Collapse Calderas Workshop IOP Publishing. IOP Conf. Ser. Earth Environ. Sci. 3, 012003. doi:10.1088/1755-1307/3/1/012003.

Guzmán, S., Petrinovic, I., 2010. The Luingo caldera: the south-easternmost collapse caldera in the Altiplano–Puna plateau, NW Argentina. J. Volcanol. Geotherm. Res. 194, 174–188.

Harmon, R.S., Barreiro, B.A., Moorbath, S., Hofes, J., Francis, P.W., Thorpe, R.S., Deruelle, B., McHugh, J., Viglino, J.L., 1984. Regional O-, Sr-, and Pb-isotope relationships in late Cenozoic calcalkaline lavas of the Andean Cordillera. J. Geol. Soc. Lond. 141, 803–822.

Heit, B., Sodoudi, F., Yuan, X., Bianchi, M., Kind, R., 2007. An S receiver function analysis of the lithospheric structure in South America. Geophys. Res. Lett. 34, L14307. doi:10.1029/2007GL030317.

Hess, J.C., Lippolt, H.J., 1994. Compilation of K–Ar measurements on HD-B1 standard biotite — 1994 status report. In: Odin, G.S. (Ed.), Phanerozoic time Scale, Bull. Liais. Inform. IUGS Subcom. : Geochronol., 12. Offset Paris, pp. 19–23.

Hoke, G., Garzione, C., 2008. Paleosurfaces, paleoelevation, and the mechanism for the late Miocene topographic development of the Altiplano Plateau. Earth Planet. Sci. Lett. doi:10.1016/j.epsl.2008.04.008.

Hongn, F. D., Seggiaro, R., 2001. Hoja Geológica 2566 – III. Cachi. Boletín N° 248. Programa Nacional de Cartas Geológicas 1:250.000. SEGEMAR, Argentina.

Hongn, F., del Papa, C., Powell, J., Petrinovic, I., Mon, R., Deraco, V., 2007. Middle Eocene deformation and sedimentation in the Puna–Eastern Cordillera transition (23°–26° S): control by preexisting heterogeneities on the pattern of initial Andean shortening. Geology 35 (3), 271–274.

Isacks, B., 1988. Uplift of the Central Andean Plateau and bending of the Bolivian Orocline. J. Geophys. Res. 93 (4), 3211–3231.

Ishizuka, O., Yuasa, M., Uto, K., 2002. Evidence of porphyry copper-type hydrothermal activity from a submerged remnant back arc volcano of the Izu-Bonin arc: implication for the volcanotectonic history of back-arc seamounts. Earth Planet. Sci. Lett. 198, 381–399.

James, D., 1971. Andean crustal and upper mantle structure. J. Geophys. Res. 76 (14), 3246–3271.

Kay, S.M., Mpodozis, C., Coira, B., 1999. Neogene magmatism, tectonism, and mineral deposits of the Central Andes 22° to 33°S latitude. In: Skinner, B.J. (Ed.), Geology and Ore Deposits of the Central Andes. : Soc. Econ. Geol., 7. Special Publication, pp. 27–59.

Kay, S.M., Coira, B., Woerner, G., Singer, B.S., 2008. Cerro Galán Ignimbrite: trace element, isotopic and 40Ar/39Ar age constraints on the evolution of the central Andean lithosphere. American Geophysical Union, Fall Meeting. 2008, abstract #V22A-06. http://adsabs.harvard.edu/abs/2008AGUFM.V22A.06K.

Kay, S.M., Coira, B., Wörner, G., Kay, R.W., Singer, B.S., 2010. Geochemical, isotopic and single crystal $^{40}Ar/^{39}Ar$ age constraints on the evolution of the Cerro Galán Ignimbrites. Bull. Volcanol. doi:10.1007/s0045-010-0410-7.

Kochhar, N., 1977. Post-emplacement alkali modifications in rapidly cooled acid volcanic rocks. Am. Mineral. 62, 333–335.

Kraemer, B., Adelmann, D., Alten, M., Schnurr, W., Erpenstein, K., Kiefer, E., van den Bogaard, P., Görler, K., 1999. Incorporation of the Paleogene foreland into the Neogene Puna Plateau, the Salar de Antofalla area, NW Argentina. J. S. Am. Earth Sci. 12, 157–182.

Leake, B.E., Wooley, A.R., Arps, C.E.S., Birch, W.D., Gilbert, M.C., Grice, J.D., Hawthorne, F.C., Kato, A., Kisch, H.J., Krivovichev, V.G., Linthout, K., Laird, J., Mandarino, J.A.,

Maresch, W.V., Nickel, E.H., Rock, N.M.S., Schumacher, J.C., Smith, D.C., Stephenson, N.C.N., Ungaretti, L., Whittaker, E.J.W., Youzhi, G., 1997. Nomenclature of amphiboles: report of the Subcommittee on Amphiboles of the International Mineralogical Association, Commission on New Minerals and Mineral Names. Am. Mineral. 82, 1019–1037.

Le Maitre, R., Baterman, P., Dudek, A., Keller, J., Lameyre Le Bas, M., Sabine, P., Schmid, R., Sorensen, H., Streckeisen, A., Woolley, A., Zanettin, B., 1989. A classification of igneous rocks and glossary of Terms. Blackwell, Oxford. 93 pp.

Lindsay, J.M., de Silva, S., Trumbull, R., Emmermann, R., Wemmer, K., 2001a. La Pacana caldera, N. Chile: a re-evaluation of the stratigraphy and volcanology of one of the world's largest resurgent caldera. J. Volcanol. Geotherm. Res. 106, 145–173.

Lindsay, J.M., Schmitt, A.K., Trumbull, R.B., DeSilva, S.L., Siebel, W., Emmermann, R., 2001b. Magmatic evolution of the La Pacana caldera system, central Andes, Chile: compositional variation of two cogenetic large-volume felsic ignimbrites. J. Petrol. 42, 459–486.

Lipman, P.W., 1965. Chemical comparison of glass and crystalline volcanic rocks. U S. Geol Surv. Bull. 1201-D, Dl–D24.

Lucassen, F., Becchio, R., Harmon, R., Kasemann, S., Franz, G., Trumbull, R., Wilke, H., Romer, R., Dulski, P., 2001. Composition and density model of the continental crust at an active continental margin — the Central Andes between 21° and 27° S. Tectonophys. 341, 195–223.

Marrett, R., Emerman, S.H., 1992. The relations between faulting and mafic magmatism in the Altiplano–Puna plateau (Central Andes). Earth Planet. Sci. Lett. 112, 53–59.

Marrett, R., Allmendinger, R., Alonso, R., Drake, R., 1994. Late Cenozoic tectonic evolution of the Puna Plateau and adjacent foreland, northwestern Argentine Andes. J. S. Am. Earth Sci. 7 (2), 179–207.

McDonough, W.F., Sun, S., 1995. The composition of the Earth. Chem. Geol. 120, 223–253.

McDougall, I., Harrison, T.M., 1999. Geochronology and Thermochronology by the $^{40}Ar/^{39}Ar$ method. New York, Oxford University Press. 269 pp.

McDowell, F.W., Clabaugh, S.E., 1979. Ignimbrites of the Sierra Madre Occidental and their relation to the tectonic history of western Mexico. In: Chapin, C.E., Elston, W.E. (Eds.), Ash-Flow Tuffs: Geol. Soc. Am. Spec. Paper 180, pp. 113–124.

Molnar, P., Garzione, C.N., 2007. Bounds on the viscosity coefficient of continental lithosphere from removal of mantle lithosphere beneath the Altiplano and Eastern Cordillera. Tectonics 26. doi:10.1029/2006TC001964.

Mon, R., Salfity, J.A., 1995. Tectonic evolution of the Andes of Northern Argentina. In: Tankard, A.J., Suárez, R., Welsink, H.J. (Eds.), Petroleum basins of South America, American Association of Petroleum Geologists, Memoir 62, pp. 269–283.

Morimoto, N., 1988. Nomenclature of pyroxenes. Am. Mineral. 73, 1123–1133.

Mortimer, E., Carrapa, B., Coutand, I., Schoenbohm, L., Sobel, E., Sosa Gómez, J., Strecker, M., 2007. Fragmentation of a foreland basin in response to out-of-sequence basement uplifts and structural reactivation: El Cajón-Campo del Arenal basin, NW Argentina. Geol. Soc. Am. Bull. 119 (5/6), 637–653.

Mpodozis, C., Cornejo, P., Kay, S.M., Tittler, A., 1995. La Franja de Maricunga: síntesis de la evolución del Frente Volcánico Oligoceno–Mioceno de la zona sur de los Andes Centrales. Rev. Geol. Chile 21 (2), 273–313.

Mpodozis, C., Arriagada, C., Basso, M., Roperch, P., Cobbold, P., Reich, M., 2005. Late Mesozoic to Paleogene stratigraphy of the Salar de Atacama Basin, Antofagasta, Northern Chile: implications for the tectonic evolution of the Central Andes. Tectonophys. 399, 125–154.

Navarro García, L., 1984. Estratigrafía de la región comprendida entre los paralelos de 26° 00′ a 26°15′ de latitud sur y los meridianos de 66° 30′a 67° 00′ de longitud oeste, Provincia de Catamarca. 9° Congreso Geológico Argentino, Actas 1, Bariloche, pp. 353–383.

Ort, M., 1993. Eruptive processes and caldera formation in a nested downsag collapse caldera: Cerro Panizos, central Andes Mountains. J. Volcanol. Geotherm. Res. 56, 221–252.

Patiño Douce, A.E., 1993. Ti substitution in biotite: an empirical model with applications to thermometry, O2 and water barometries, and consequences for biotite stability. Chem. Geol. 108, 133–162.

Pearce, J.A., 1983. Role of the sub-continental lithosphere in magma genesis at active continental margins. In: Hawkesworth, C.J., Norry, M.J. (Eds.), Continental Basalts and Mantle Xenoliths. Nantwich, pp. 230–249.

Petrinovic, I.A., Martí, J., Aguirre-Díaz, G.J., Guzmán, S.R., Geyer, A., Salado Paz, N., 2010. The Cerro Aguas Calientes caldera, NW Argentina: an example of a tectonically controlled polygenetic collapse caldera, and its regional significance. J. Volcanol. Geotherm. Res. 194, 15–26.

Riller, U., Oncken, O., 2003. Growth of the central Andean plateau by tectonic segmentation is controlled by the gradient in crustal shortening. J. Geol. 111, 367–384.

Saunders, A.D., Tarney, J., 1984. Geochemical characteristics of basaltic volcanism within back-arc basins. In: Kokelaar, B.P., Howells, M.F. (Eds.), Marginal Basin Geology. Geol. Soc. Special Publication, London, pp. 59–76. 16.

Schnurr, W., Trumbull, R., Clavero, J., Hahne, K., Siebel, W., Gardeweg, M., 2007. Twenty-five million years of silicic volcanism in the southern central volcanic zone of the Andes: geochemistry and magma genesis of ignimbrites from 25 to 27° S, 67 to 72° W. J. Volcanol. Geotherm. Res. 166, 17–46.

Inversión Tectónica del Cerro Colorado, Departamento San Carlos, Provincia de Salta. 13° Reunión de Tectónica. Abstracts, San Luis, Argentina.

Sempere, T., Buttle, R., Richards, D.R., Marshall, L.G., Sharp, W., Swisher, C.C.L., 1997. Stratigraphy and chronology of Late Cretaceous–early Paleogene strata in Bolivia and northwest Argentina. Geol. Soc. Am. Bull. 109, 709–727.

Siebel, W., Schnurr, W., Hahne, K., Kraemer, B., Trumbull, R., van den Bogaard, P., Emmermann, R., 2001. Geochemistry and isotope systematics of small to medium volume Neogene Quaternary ignimbrites in the southern central Andes: evidence for derivation from andesitic magma sources. Chem. Geol. 171, 213–217.

Smith, R.L., 1960. Ash flows. Geol. Soc. Am. Bull. 71, 795–842.

Soler, M.M., 2005. Caldera Vilama (Mioceno Superior): su estratigrafía, evolución magmática y relación con eventos ignimbríticos tempranos. Puna Argentina–Altiplano Boliviano. PhD Thesis, Universidad Nacional de Salta, Argentina

Soler, M.M., Caffe, P.J., Coira, B.L., Onoe, A.T., Kay, S.M., 2007. Geology of the Vilama caldera: a new interpretation of a large-scale explosive event in the Central Andean plateau during the Upper Miocene. J. Volcanol. Geotherm. Res. 164 (1–2), 23–53.

Sparks, R., Francis, P., Hamer, R., Pankhurst, R., O'Callaghan, L., Thorpe, R.S., Page, R., 1985. Ignimbrites of the Cerro Galán caldera, NW Argentina. J. Volcanol. Geotherm. Res. 24, 205–224.

Streck, M., 2008. Mineral textures and zoning as evidence for open system processes. Rev. Mineral. Geochem. 69, 595–622.

Strecker, M., Alonso, R., Bookhagen, B., Carrapa, B., Hilley, G., Sobel, E., Trauth, M., 2007. Tectonics and climate of the Southern Central Andes. Ann. Rev. Earth Planet. Sci. 35, 747–787.

Sudo, M., Uto, K., Anno, K., Ishizuka, O., Uchiumi, S., 1998. SORI93 biotite: a new mineral standard for K–Ar dating. Geochem. J. 32, 49–58.

Thorpe, R.S., Francis, P.W., O'Callaghan, L.O., 1984. Relative roles of source composition, fractional crystallization and crustal contamination in the petrogenesis of Andean volcanic rocks. Philos. Trans. R. Soc. Lond. 310, 675–692.

Tischendorf, G., Gottesmann, B., Förster, H.J., Trumbull, R.B., 1997. On Li-bearing micas: estimating Li from electron microprobe analyses and improved diagram for graphical representation. Mineral. Mag. 61, 809–834.

Tomiya, A., Takahashi, E., 2005. Evolution of the magma chamber beneath Usu Volcano since 1663: a natural laboratory for observing changing phenocryst compositions and textures. J. Petrol. 46 (12), 2395–2426.

Trumbull, R., Wittenbrink, R., Hahne, K., Emmermann, R., Büsch, W., Gerstenberger, H., Siebel, W., 1999. Evidence for Late Miocene to Recent contamination of arc andesites by crustal melts in the Chilean Andes (25–26°S) and its geodynamic implications. J. S. Am. Earth Sci. 12, 135–155.

Uto, K., Ishizuka, O., Matsumoto, A., Kamioka, H., Togashi, S., 1997. Laser-heating $^{40}Ar/^{39}Ar$ dating system of the Geological Survey of Japan: system outline and preliminary results. Bull. Geol. Surv. Jpn 48, 23–46.

Wones, D.R., 1970. Amphibole–biotite relations. Am. Mineral. 55, 295–296.

Yavutz, F., 2001. LIMICA: a program for estimating Li from electron-microprobe mica analyses and classifying trioctahedral micas in terms of composition and octahedral site occupancy. Comput. Geosci. 27, 215–227.

Yuan, X., Sobolev, S.V., Kind, R., 2002. Moho topography in the Central Andes and its geodynamics implications. Earth Planet. Sci. Lett. 199, 389–402.

Yuan, X., Sobolev, S.V., Kind, R., Oncken, O., Bock, G., Asch, G., Schurr, B., Graeber, F., Rudloff, A., Hanka, W., Wylegalla, K., Tibi, R., Haberland, C., Rietbrock, A., Giese, P., Wigger, P., Röwer, P., Zandt, G., Beck, S., Wallace, T., Pardo, M., Comte, D., 2000. Subduction and collision processes in the Central Andes constrained by converted seismic phases. Nature 408, 958–961.